Energy-Harvesting Aided Unmanned Aerial Vehicles for Reliable Ground User Localization and Communications Under Lognormal-Nakagami-m Fading Channels

Ngoc Phuc Le[†#], Le Chung Tran[#], Xiaojing Huang[*], Eryk Dutkiewicz[*], Christian Ritz[#], Son Lam Phung[#], Abdesselam Bouzerdoum[&#], Daniel Franklin[*] and Lajos Hanzo[‡]

Abstract—In this paper, we propose a wireless localization system based on energy-harvesting aided unmanned aerial vehicles (UAV). Our proposed system consists of a ground station (GS), a UAV, and multiple users located on the ground, in which both the ground station and all the ground users (GUs) want to know the locations of the ground users. To this end, the UAV first harvests energy from the GS, and then broadcasts signals to the GUs for localization. Each GU will estimate its location, and then transmits data, including its location information, to the GS with the help of the UAV. The links between nodes experience both large-scale lognormal shadowing and small-scale Nakagami-m fading. We first derive the Cramer-Rao lower bound (CRLB) under spatially correlated shadowing for localization performance evaluation. Next, we analyze the system throughput under delay-limited and delay-tolerant transmission modes. To derive exact closed-form expressions as well as high signal-to-noise ratio (SNR) approximations of the performance metrics, we consider a mixture gamma distribution approximation for the probability density functions (PDF) of the composite fading channels. We evaluate the impact of several key system parameters such as the number of waypoints and the altitude of the UAV, correlated shadowing and energy-harvesting time both on the localization performance and on the achievable throughput. Simulations are provided to validate the theoretical analysis.

Index Terms—Energy harvesting, unmanned aerial vehicle (UAV), localization, Cramer-Rao lower bound, throughput, lognormal-Nakagami-m fading.

I. INTRODUCTION

Localization has become an important research area due to the popularity of wireless sensor networks and location-based services. Location-aware communications, disaster managements, search and rescue missions, and military operations are among critical localization applications [1]. In 5G and beyond 5G networks, it is envisioned that wireless localization plays an essential role for both human-centric communications and machine-type communications [2], [3]. It is well-known that the global positioning system (GPS) is an efficient solution for outdoor localization. However, GPS does not work reliably in indoor environments or under harsh conditions (e.g., forest environments) since satellite signals are severely attenuated. Furthermore, GPS signals can be easily jammed due to its low signal intensity. Consequently, alternative localization techniques have been extensively studied in the literature [4].

Non-GPS localization schemes can be categorized into range-free and range-based schemes. Range-free methods work on attributes that approximate the distances, such as hop count, whereas range-based approaches estimate the absolute distances [4]. At the expense of requiring a dedicated infrastructure, range-based methods can achieve higher accuracy than their counterparts. Diverse techniques are suitable for range estimation, relying on Time of Arrival (TOA), Time Difference of Arrival (TDOA), Angle of Arrival (AOA), and Received Signal Strength (RSS). Among these techniques, the RSS is particularly attractive due to its intrinsic simplicity, requiring no extra antennas or time synchronization [5], [6]. In the RSS method, the relationship between the received signal strength indicator and the distance between an anchor and a target object is obtained based on the path-loss [6]. The RSS-based estimator may rely on full-search based maximum likelihood (ML) [7] or suboptimal least square (LS) techniques [8]. The RSS-based localization using terrestrial anchors has also been widely investigated in the literature [5], [6]. Furthermore, several research contributions studied RSS-based localization using mobile anchors [5], [9]. The impact of spatial correlation between anchors on the localization performance was examined in [10].

In recent years, unmanned aerial vehicles (UAVs), also known as drones, have attracted substantial attention due to their potential for future wireless communications [11], [12]. In general, UAV-based wireless networks may be promptly rolled out and can enjoy excellent channel conditions due to the presence of line-of-sight (LoS) links. Typical application scenarios of UAV-aided wireless communications include UAV-aided ubiquitous coverage, UAV-assisted relaying and UAV-aided information dissemination as well as data collection [12]. However, one of the main concerns for the deployment of UAVs is the limited energy available to sustain their operations. Concurrently, energy-harvesting has been shown as a promising solution to prolong the lifetime of energy-constrained wireless networks [13], [14]. In fact, energy-harvesting has been studied for many types of wireless systems, such as multiple-input multiple-output (MIMO)

schemes [15], multiuser systems [16], relay systems [17] and cognitive relay networks [18]. Motivated by this, researchers have considered wireless power transfer to sustain the UAVs' recharge period [19]-[23]. These research activities include their performance analysis [20], [21] as well as the joint optimization of time and power allocation in energy-harvesting UAV communications [22], [23]. As a compelling design alternative, laser guns placed on rooftops could be used for replenishing the batteries [24].

A. Related Contributions on UAV-based RSS Localization and Open Problems

Recently, some authors have considered aerial anchors, such as UAVs, for terrestrial object localization [25]-[32]. In particular, Gong et al. [25] proposed a localization framework which employs a mobile node to serve as a virtual anchor. They implemented it on a UAV to verify the reliability of the proposed system. Sallouha et al. [26] considered multiple UAVs for outdoor localization in urban environments. They investigated the optimal altitude for localization accuracy under a LoS and non-LoS (NLoS) mixed channel model. They also derived the Cramer Rao lower bound (CRLB) for quantifying the impact of the UAV altitude on the localization error. However, it is worth noting that the CRLB derivation in their study is limited to a performance metric relying on individual range estimators. Localization algorithms with improved precision were developed by Sorbelli et al. [27] using both directional and omnidirectional antennas. The ground nodes calculated their own positions through trilateration based on the measurements received from the UAV.

With respect to the UAV trajectory design of localization systems, Perazzo et al. [28] considered path planning based on the traveling salesman problem for a UAV to localize the objects' positions using round trip time for distance estimation which requires reliable timing. In [29], Shahidian et al. proposed two trajectory control approaches by applying the extended Kalman filter to increase the localization accuracy. Trajectory planning was designed by Ji et al. [30] for multi-target positioning using multiple UAVs who minimized the energy dissipation of UAVs performing cooperative positioning via trilateration. Demiane et al. [31] designed an efficient UAV trajectory that takes into account important levels of objects in disaster scenarios. Furthermore, a reinforcement learning technique has been adopted by Ebrahimi et al. [32] for UAV trajectory design to localize ground objects, which was shown to be superior to the existing methods regarding localization errors under a fixed amount of UAV energy consumption, path length and flying time.

However, the aforementioned contributions only consider localization performed either at ground users or at UAVs, which is hence only known by either the ground users or UAVs, even though in many practical scenarios, it is required by both as well as by the central station. To fill this knowledge gap, a joint localization and communications study is essential. Also, as discussed earlier, the limited energy supplied by an onboard battery may be replenished by energy harvesting. Additionally, it is highly likely that there exists spatially correlated shadowing between UAVs or among waypoints of a particular UAV due to the inherent characteristics of UAV's flying environments. Therefore, it is necessary to consider the impact of shadowing correlation on UAV-based localization systems. These concerns will be addressed in this work.

B. Paper Contributions and Structure

In this paper, we consider energy-harvesting UAV based wireless localization systems, where each ground user (GU) wants to locate its position. The ground base station (GS) also wants to know the locations and data of several ground users. We consider scenarios where the GS is located far from the GUs or blocked by man-made or natural structures. Therefore, there is no direct signal transmission from the GUs to the GS. To accomplish its mission, the UAV is responsible both for localization and information transfer. We assume that the UAV is an energy-limited device and thus it has to harvest energy from the GS for its communication tasks. The GUs estimate their location using the RSS based on signals broadcast by the UAV from different waypoints. Our contributions are:

1) We propose and analyse a new energy-harvesting UAV-based system for joint wireless localization and communications, rather than considering the mature conceived problem of a stand-alone localization scheme. Specifically, we investigate both the performance of the localization operations performed at the GUs and the information transmission of the GUs' locations forwarded to the GS via the UAV. To this end, we analyze the localization performance at the GUs under shadowing-induced correlation as well as the outage probability and the achievable throughput at the GS. A summary of system characteristics considered in this paper versus the related contributions is provided in Table I.
2) We propose an analytical approach for UAV-based systems by using a mixture gamma distribution approximation. This novel method allowed us to derive insightful new closed-form expressions of the key system metrics, including the outage probability (OP) and throughput (TP), when composite fading channels (i.e., lognormal-Nakagami-m fading) are used to model the GU-UAV and UAV-GS links. Both *delay-limited* and *delay-tolerant* transmission modes are investigated. Consequently, the results obtained can be applied to a wide range of channel models, including lognormal-Nakagami-m, K_G, $\eta - \mu$, Nakagami-q (Hoyt), $\kappa - \mu$, Nakagami-n (Rician), Nakagami-m, and Rayleigh channels.

The main results of this paper are summarized below.
- The Cramer-Rao lower bound (CRLB) of location estimation is derived under spatially correlated shadowing environments. The expression derived reveals the effects of several key parameters on the bound, thus facilitating the system design and the evaluation of localization performance.
- The throughput attained by the ground station is analyzed. In particular, we calculate the OP and TP for a delay-limited mode. We also derive the exact closed-form expressions for the ergodic capacity and throughput

TABLE I: Related contributions versus this paper on UAV-based localization.

	[25] 2017	[26] 2018	[27] 2018	[28] 2017	[29] 2017	[30] 2020	[31] 2020	[32] 2020	This work
Localization technique	RSS	RSS	RSS	RSS	RSS	RSS	RSS	RSS	RSS
Localization algorithm	Newton iteration method	Maximum likelihood	Tri-lateration	Tri-lateration	Extended Kalman filter	Tri-lateration	Tri-lateration	Reinforcement learning	Maximum likelihood
Channel model	log-distance path loss model (LPL)	Probabilistic LoS/N-LoS	LPL	LPL	LPL	LPL	LPL	Probabilistic LoS/N-LoS	LPL and log-normal Nakagami-m fading channel
Correlated shadowing									✓
Energy-harvesting									✓
CRLB Derivation	✓	✓(only for individual distance)			✓				✓
UAV trajectory	uniformly distributed	3 UAVs forming a triangle	predefined path	design trajectory	design trajectory	design trajectory	design trajectory	design trajectory	regular-polygon
Impact of UAV waypoints	✓	✓	✓		✓	✓	✓	✓	✓
Impact of UAV altitude	✓	✓	✓				✓	✓	✓
Joint communication and localization									✓

in a delay-tolerant transmission. In addition, we derive approximate expressions for both the OP and the TP at high SNRs.

- The optimal energy-harvesting time achieved the maximum throughput in the system is obtained.
- The effects of the number of waypoints, of the UAV altitude, of the spatially correlated shadowing and of the energy-harvesting time both on the localization performance and on the system throughput are evaluated.

The rest of the paper is organized as follows. Section II describes the proposed UAV-based localization system model, whereas Section III analyzes the ML estimator and the CRLB. In Section IV, we derive the system throughput in both delay-limited and delay-tolerant transmission modes. Our simulation results and discussions are provided in Section V. Finally, Section VI concludes the paper.

Notation: Throughout this paper, a bold letter denotes a vector or matrix, whereas an italic letter denotes a variable; $(\cdot)^T$, and $\mathbb{E}\{\cdot\}$ indicate transpose and expectation, respectively; $\Gamma(x)$ and $\gamma(x, \lambda)$ are the gamma function and lower incomplete gamma function, respectively [33, Eq. (8.310.1),(8.350.1)]; $K_\nu(x)$ is the ν-*th* order modified Bessel function of the second kind [33, Eq. (8.407.1)]; $\psi(\cdot)$ is the Euler Psi function [33, Eq. (8.360.1)]; and $G_{p,q}^{m,n}(\cdot)$ is the Meijer G-function [33, Eq. (9.301)].

II. ENERGY-HARVESTING UAV LOCALIZATION SYSTEM MODEL

We consider an energy-harvesting UAV localization system that consists of a ground station (GS), a UAV, and I ground users (GUs), as shown in Figure 1. All nodes are equipped with a single antenna. All GUs are distributed randomly within a particular area. We assume that the direct links between the GS and the GUs are weak due to obstacles and/or poor channel conditions. Consequently, information is transferred

from the GUs to the GS with the help of the UAV. Here, we are interested in the deployment of only a single UAV, instead of multiple UAVs for having a cost-effective implementation. Additionally, the system complexity is low since no information coordination is required among multiple UAVs. However, it is worth noting that the results in this work are applicable to the scenarios of multiple UAVs as well. In this contribution, we consider situations that a UAV scavenges energy from external sources for extending its continuous operation without landing to recharge or replace its battery. To this end, we consider wireless power transfer (WPT) for a UAV. The current status and potential of WPT for powering UAVs was discussed in [19], and our work is in line with advanced research papers, where a charging station is used for wirelessly powering UAVs [19]-[23]. The position of the GS is defined as $(x_b, y_b, 0)$, while the locations $(x_i, y_i, 0), i = 1, 2, ..., I$, of the GUs are denoted as $\mathcal{L}_i = (x_i, y_i)^T$. The UAV flies along its predefined trajectory at the height of h through K waypoints. Its position is denoted as $(x_k, y_k, h), k = 1, 2, ..., K$. The proposed system protocol is depicted in Figure 2. The detailed system operations are described in the next subsections.

A. Air-to-Ground Channel Model

We adopt a channel model in which the channel gains are dominated by light-of-sight (LoS) links and the Doppler effect is accurately compensated. Note that this channel model matches well with practical measurements [34]. To generalize our analysis, we consider Nakagami-m fading for small-scale fading effects, and lognormal shadowing for large-scale effects. In particular, for the UAV-GS link, the multipath channel coefficient is denoted by h_{ub}, with its envelope $|h_{ub}|$ following an independent and identically distributed (i.i.d) Nakagami-m distribution having the parameter m_{ub} and squared mean of $\Omega_{ub} = \mathbb{E}\{|h_{ub}|^2\} = 1$. Similarly, small-scale fading channel coefficients for the GU-UAV links are

TABLE II: Notations for channel links.

Channel links	Label[(1)]	Distance-based path gain	Large-scale fading	Small-scale fading
$GS \rightarrow UAV$	bu	$G_{bu} = g_{0,b}/d_{ub}^{\beta}$	$S_{bu} \sim$ lognormal$(\mu_{ub}, \sigma_{ub}^2)$	$H_{bu} \sim$ Nakagami-m
$UAV \rightarrow GS$	ub	$G_{ub} = g_{0,u}/d_{ub}^{\beta}$	$S_{ub} \sim$ lognormal$(\mu_{ub}, \sigma_{ub}^2)$	$H_{ub} \sim$ Nakagami-m
$GU(i^{th}) \rightarrow UAV(k^{th})$	ou	$G_{ou} = g_{0,o}/d_{i,k}^{\beta}$	$S_{ou,i}^k \sim$ lognormal$(\mu_{ou}, \sigma_{ou}^2)$	$H_{ou,i}^k \sim$ Nakagami-m
$UAV(k^{th}) \rightarrow GU(i^{th})$	uo	$G_{uo} = g_{0,u}/d_{i,k}^{\beta}$	$S_{uo,i}^k \sim$ lognormal$(\mu_{ou}, \sigma_{ou}^2)$	$H_{uo,i}^k \sim$ Nakagami-m

(Note: b: base station; u: uav; o: object)

$h_{ou,i}^k, (i = 1, 2, ..., I; k = 1, 2, ..., K)$. Thus, the small-scale channel power gains are $H_{ub} = |h_{ub}|^2$ and $H_{ou,i}^k = |h_{ou,i}^k|^2$. For large-scale fading, S_{ub} denotes the lognormal variable that accounts for shadowing variation of the UAV-GS links, where the mean and variance of the associated Gaussian process of the shadowing expressed in dB are μ_{ub} and σ_{ub}^2, respectively. Similarly, $S_{ou,i}^k$ represents the GU-UAV links between the ith ground user with the kth waypoint with the mean $\mu_{i,k}$ and variance $\sigma_{i,k}^2$. For simplicity, we assume that all GU-UAV links have the same mean and variance, i.e., $\mu_{i,k} = \mu_{ou}$ and $\sigma_{i,k}^2 = \sigma_{ou}^2, \forall i, k$. Additionally, the path loss exponent of the links is denoted as β. Therefore, a distance-based path gain between the UAV and the GS when the UAV hovers at the first waypoint can be expressed as[1]

$$G_{ub} = \frac{g_{0,u}}{d_{ub}^{\beta}} = \frac{g_{0,u}}{(\text{h}^2 + [(x_b - \text{x}_1)^2 + (y_b - \text{y}_1)^2])^{\beta/2}}, \quad (1)$$

where $g_{0,u}$ is the reference gain of the UAV at the reference distance of 1 meter, and $d_{ub} = \sqrt{\text{h}^2 + [(x_b - \text{x}_1)^2 + (y_b - \text{y}_1)^2]}$ is the distance between the GS and the first waypoint. Similarly, the distance-based path gain between the ith GU and the kth waypoint is

$$G_{ou,i}^k = \frac{g_{0,o}}{d_{i,k}^{\beta}} = \frac{g_{0,o}}{(\text{h}^2 + [(x_i - \text{x}_k)^2 + (y_i - \text{y}_k)^2])^{\beta/2}}. \quad (2)$$

Here, $g_{0,o}$ is the reference gain of the ith GU, which is assumed to be the same for all ground users, and $d_{i,k} = \sqrt{\text{h}^2 + [(x_i - \text{x}_k)^2 + (y_i - \text{y}_k)^2]}$ is the distance between the ith GU and the kth waypoint. A summary of notations for channel modeling is given in Table II. Note that the large-scale and small-scale fadings of the forward and reverse links between the GS and the UAV have the same mean and variance values, i.e., $\mu_{bu} = \mu_{ub}$, $\sigma_{bu}^2 = \sigma_{ub}^2$, and $m_{bu} = m_{ub}$. Meanwhile, the difference in terms of a distance-based path gain (i.e., G_{bu} and G_{ub}) is due to the difference in the reference gains between $g_{0,b}$ and $g_{0,u}$, e.g., their transmit antenna gains are different. A similar observation applies for the link between the GU and the UAV. Additionally, the overall instantaneous channel gain is a superposition of the three types of gains mentioned above. As an example, the instantaneous channel gain for a transmission session from the ith GU to the kth waypoint of the UAV is $G_{ou,i}^k S_{ou,i}^k H_{ou,i}^k$.

B. Energy-Harvesting Phase

As shown in Figure 2, the UAV harvests energy from the GU during the time period of $(1 - \alpha)T, 0 < \alpha < 1$, when it

[1]Note that since we assume that the UAV only communicates with the GS when it hovers at the first waypoint, the index k is dropped for simplicity.
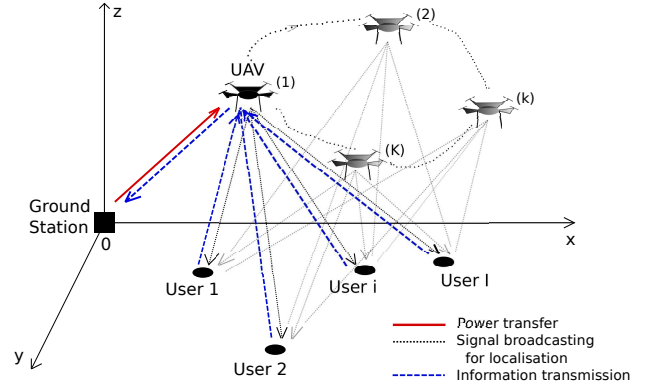

Fig. 1: An energy-harvesting UAV based localization system model.
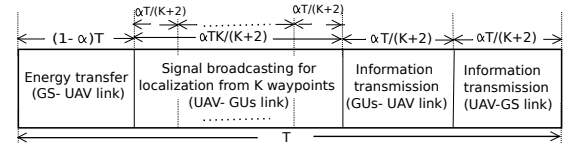

Fig. 2: A proposed protocol for localization and information transmission.

hovers at the first waypoint. The averaged harvested energy can be expressed by [15]-[18]

$$E_u = \eta P_b(1 - \alpha)TG_{bu}S_{bu}, \quad (3)$$

where $\eta, 0 \leq \eta \leq 1$, is the energy conversion efficiency, and P_b is the transmit power of the GS. The UAV will use this amount of energy for its communications tasks, including broadcasting signals to all the GUs from K waypoints and forwarding signals from the GUs to the GS[2]. We assume equal energy allocation for each transmission session. Thus, the energy allocated for each transmission session is $E_u/(K+1)$. Consequently, the transmit power for each operation is expressed as

$$P_u = \frac{E_u/(K + 1)}{\alpha T/(K + 2)} = \frac{(K + 2)(1 - \alpha)\eta P_b G_{bu}S_{bu}}{(K + 1)\alpha}. \quad (4)$$

C. Localization Phase

After harvesting sufficient energy from the GS, the UAV starts to broadcast signals to the GUs. The UAV will fly along its trajectory and hover at each waypoint to broadcast signals.

[2]The power required for propulsion depends on the specific type and the size of the UAV [35]. A helium-filled tethered UAV does not need any propulsion power at all, but naturally quadcopters need power for propulsion. Indeed, for the latter case, a large amount of harvested-energy is required, which can be delivered by adopting energy beamforming from a high-power charging station, using a high tower for low-altitude UAVs. Finally, laser beams relying on laser-guns at roof-tops may be employed [24], [36].

The time-average signal power received at the ith GU when the UAV transmits at the kth waypoint, $k = 1, 2, ..., K$, is

$$P_i^k = P_u G_{uo,i}^k S_{uo,i}^k = \frac{(K+2)(1-\alpha)\eta P_b G_{bu} G_{uo,i}^k S_{bu} S_{uo,i}^k}{(K+1)\alpha}. \quad (5)$$

After obtaining K measurements $P_i^k, k = 1, 2, ..., K$, the ith GU will estimate its location by using range-based methods. In this study, the maximum likelihood (ML) estimation is adopted for attaining the best possible result and for validating the CRLB expression derived in Section III. Note that to estimate the position of an object in the three-dimensional space, at least four reference signals are required. When a target object is located on the ground, as in the case of our system model, at least three waypoints are needed for localization, requiring $K \geq 3$. Here, the positions of the K waypoints of the UAV and the UAV transmit power value of P_u may be predefined or signalled to the GUs by the UAV's broadcast signals.

D. Information Transmission Phase

Each GU, after finishing its localization calculations, will transmit its information to the GS on its channel via the UAV, which includes the estimated location of the GU, together with other information that the user wants to report to the GS.

We assume that the UAV returns to the first waypoint after it has traveled along its entire path and it remains hovering at this waypoint during the information transmission phase. Thus, the instantaneous received SNR at the UAV for the data transmitted by the ith GU can be expressed as

$$\gamma_{ou,i} = \frac{P_{o,i} G_{ou,i}^1 S_{ou,i}^1 H_{ou,i}^1}{N_0}, \quad (6)$$

where $P_{o,i}$ is the transmit power of the ith GU and N_0 is the variance of the additive white Gaussian noise (AWGN). Given that a decode-and-forward (DF) relaying protocol is adopted, the UAV will decode the received signal and then transmit it to the GS [3]. In case of $\gamma_{ou,i}$ being smaller than a threshold γ_{th}, an outage will occur at the UAV. Note that the transmit power allocated for forwarding information for each GU is P_u/I. At the GS, the received SNR for the signal transmitted from the UAV associated with the data of the ith GU is (cf.(3))

$$\gamma_{ub,i} = \frac{(P_u/I) G_{ub} S_{ub} H_{ub}}{N_0}$$
$$= \frac{(K+2)(1-\alpha)\eta P_b G_{bu} G_{ub} S_{bu} S_{ub} H_{ub}}{(K+1)\alpha I N_0}. \quad (7)$$

Consequently, the OP associated with the data transmission from the ith GU is formulated as

$$P_{out,i}(\gamma_{th}) = Pr(\gamma_{ou,i} < \gamma_{th}) + Pr(\gamma_{ub,i} < \gamma_{th}, \gamma_{ou,i} \geq \gamma_{th}). \quad (8)$$

[3]In our system model, both DF and amplify-and-forward (AF) relaying protocols can be adopted at the UAV. However, we are interested in scenarios that both the GS and the UAV want to know the positions of the GUs. Unfortunately, AF relaying is less suitable for this application because an AF relay node simply amplifies and retransmits the signal without decoding. Thus, DF is adopted at the UAV.

The OP of the whole system is

$$P_{out,\Sigma}(\gamma_{th}) = 1 - \prod_{i=1}^{I} [1 - P_{out,i}(\gamma_{th})]. \quad (9)$$

III. MAXIMUM LIKELIHOOD ESTIMATION AND CRAMER-RAO LOWER BOUND (CRLB) ANALYSIS

A. Maximum Likelihood Estimation

The received power at the ith GU corresponding to the kth waypoint obtained in (5) can expressed in dB as [37]

$$P_i^{k[dB]} = -10\beta \log_{10}(d_{i,k}) + \Psi_i^k + S_{uo,i}^{k[dB]}, \quad (10)$$

where $\Psi_i^k \triangleq 10\log_{10}\left(\frac{(K+2)(1-\alpha)\eta P_b S_{bu} g_{0,b} g_{0,u}}{(K+1)\alpha}\right) - 10\beta \log_{10}(d_{ub})$ and $S_{uo,i}^{k[dB]}$ is a normal distribution with variance of σ_{ou}^2 (in dB). The ML estimator will estimate the position of the ith GU via [38]

$$\hat{\mathcal{L}}_i = \arg\min_{\mathcal{L}_i}(\mathbf{P}_i - \boldsymbol{\Theta}_i)^T \boldsymbol{\Lambda}_i^{-1}(\mathbf{P}_i - \boldsymbol{\Theta}_i), \quad (11)$$

where $\hat{\mathcal{L}}_i = (\hat{x}_i, \hat{y}_i)^T$ is the estimated position, $\mathbf{P}_i \triangleq [P_i^1 \ P_i^2 \ ... \ P_i^K]^T$, $\boldsymbol{\Theta}_i$ is the mean vector, whose the kth element is $[\boldsymbol{\Theta}_i]_k \triangleq -10\beta \log_{10}(d_{i,k}) + \Psi_i^k$, and $\boldsymbol{\Lambda}_i$ is the covariance matrix of correlated shadowing variables associated with the ith GU. The off-diagonal element $(m,n), 1 \leq m, n, \leq K$ of the covariance matrix $\boldsymbol{\Lambda}_i$ is defined as $\sigma_{ou}^2 \rho_{m,n}$, where $\rho_{m,n} \in [0, 1]$ is the correlation coefficient between the mth and n^{th} RSS measurements. In line with [10], we assume that $\rho_{m,n} = \rho, \forall m, n$ for simplicity. Thus, the inverse of the matrix $\boldsymbol{\Lambda}_i$ is obtained as

$$\boldsymbol{\Lambda}_i^{-1} = \frac{1}{[1 + (K-2)\rho - (K-1)\rho^2]\sigma_{ou}^2} \times$$
$$\begin{bmatrix} (K-2)\rho+1 & -\rho & \cdots & -\rho \\ -\rho & (K-2)\rho+1 & \cdots & -\rho \\ \vdots & \vdots & \ddots & \vdots \\ -\rho & -\rho & \cdots & (K-2)\rho+1 \end{bmatrix}. \quad (12)$$

Therefore, the problem in (11) is rewritten as

$$\hat{\mathcal{L}}_i = \arg\min_{\mathcal{L}_i}\left\{ \sum_{k=1}^{K} \left([(K-2)\rho+1](P_i^k - [\boldsymbol{\Theta}_i]_k)^2 \right. \right.$$
$$\left. \left. -\rho \times \sum_{n=1,n\neq k}^{K} (P_i^k - [\boldsymbol{\Theta}_i]_k)(P_i^n - [\boldsymbol{\Theta}_i]_n) \right) \right\}. \quad (13)$$

This problem can be solved by the quasi-Newton method [38].

B. Analysis of Cramer-Rao Lower Bound

To calculate the lower limit for the variance of any unbiased estimator, the Crame-Rao Lower Bound (CRLB) is usually considered [38]. Let $\mathcal{L}_i = (x_i, y_i)^T$ be the real position of the ith GU. We can express the probability density function (PDF) of $P_i^{k[dB]}$ defined in (10) conditioned on $\mathcal{L}_i$ as

$$f_{P_i^k}(p_i^k|\mathcal{L}_i) = \frac{1}{\sqrt{2\pi\sigma_{uo}^2}} e^{-\frac{(p_i^k - [\boldsymbol{\Theta}_i]_k)^2}{2\sigma_{uo}^2}}, \quad (14)$$

In case of no shadowing correlation among the waypoints of the UAV, the joint PDF of K independent measurements at the ith GU can be expressed as

$$f_{\mathbf{P}_i}(\mathbf{p}_i|\mathcal{L}_i) = \prod_{k=1}^{K} f_{P_i^k}(p_i^k|\mathcal{L}_i) = \prod_{k=1}^{K} \frac{1}{\sqrt{2\pi\sigma_{uo}^2}} e^{-\frac{(p_i^k - [\Theta_i]_k)^2}{2\sigma_{uo}^2}}, \quad (15)$$

where $\mathbf{p}_i \triangleq [p_i^1 \ p_i^2 \ ... \ p_i^K]^T$.

In many practical scenarios, the shadowing-induced correlation coefficients are as high as 0.2 for indoor and 0.8 for outdoor [10]. The PDF for a multivariate Gaussian random variable is given by [38]

$$f_{\mathbf{P}_i}(\mathbf{p}_i|\mathcal{L}_i) = \frac{1}{(2\pi)^{K/2}|\mathbf{\Lambda}_i|^{1/2}} e^{-\frac{1}{2}(\mathbf{p}_i - \Theta_i)^T \mathbf{\Lambda}_i^{-1}(\mathbf{p}_i - \Theta_i)}, \quad (16)$$

where $|\mathbf{\Lambda}_i|$ is the determinant of $\mathbf{\Lambda}_i$.

The covariance matrix associated with the location estimation can be formulated as

$$\mathcal{C}_{\mathcal{L}_i}(\hat{\mathcal{L}}_i) = \mathbb{E}_{\mathcal{L}_i}\{(\hat{\mathcal{L}}_i - \mathcal{L}_i)(\hat{\mathcal{L}}_i - \mathcal{L}_i)^T\} = \begin{bmatrix} \sigma_{\hat{x}_i}^2 & \sigma_{\hat{x}_i\hat{y}_i} \\ \sigma_{\hat{y}_i\hat{x}_i} & \sigma_{\hat{y}_i}^2 \end{bmatrix},$$
$$(17)$$

where $\mathbb{E}_{\mathcal{L}_i}\{.\}$ is the expectation conditioned on $\mathcal{L}_i$. Note that the diagonal elements in (17) are the mean squared errors between the estimated and real positions. The CRLB is then given by [38]

$$\mathcal{C}_{\mathcal{L}_i}(\hat{\mathcal{L}}_i) \geq [\mathbf{F}(\mathcal{L}_i)]^{-1}, \quad (18)$$

where $\mathbf{F}(\mathcal{L}_i)$ is the Fisher information matrix defined as

$$\mathbf{F}(\mathcal{L}_i) = \begin{bmatrix} F_{x_i x_i}(\mathcal{L}_i) & F_{x_i y_i}(\mathcal{L}_i) \\ F_{y_i x_i}(\mathcal{L}_i) & F_{y_i y_i}(\mathcal{L}_i) \end{bmatrix}. \quad (19)$$

The calculations of the elements of this matrix are provided in Appendix A.

Let us denote the variance of the location estimate for the ith GU by $var_{\mathcal{L}_i}(\hat{\mathcal{L}}_i)$. It is seen from (18) that the matrix $\mathcal{C}_{\mathcal{L}_i}(\hat{\mathcal{L}}_i) - [\mathbf{F}(\mathcal{L}_i)]^{-1}$ is positive semidefinite. For any unbiased estimation, we arrive at

$$var_{\mathcal{L}_i}(\hat{\mathcal{L}}_i) = \sigma_{\hat{x}_i}^2 + \sigma_{\hat{y}_i}^2 \geq [\mathbf{F}(\mathcal{L}_i)]_{1,1}^{-1} + [\mathbf{F}(\mathcal{L}_i)]_{2,2}^{-1}$$
$$= \frac{F_{x_i x_i}(\mathcal{L}_i) + F_{y_i y_i}(\mathcal{L}_i)}{|\mathbf{F}(\mathcal{L}_i)|}, \quad (20)$$

where $|\mathbf{F}(\mathcal{L}_i)| = F_{x_i x_i}(\mathcal{L}_i)F_{y_i y_i}(\mathcal{L}_i) - F_{x_i y_i}(\mathcal{L}_i)F_{y_i x_i}(\mathcal{L}_i)$. After some further manipulations, we obtain the expression for the CRLB.

Theorem 1. *The CRLB for the estimated location of the ith GU under spatially correlated shadowing is given by (21) (on the top of this page), where $X_{i,k} \triangleq (x_i - \mathrm{x}_k)/d_{i,k}^2$, $Y_{i,k} \triangleq (y_i - \mathrm{y}_k)/d_{i,k}^2$, K is the number of waypoints, ρ is the correlation coefficient, β is the path-loss exponent and σ_{ou}^2 is the lognormal shadowing variance.*

Proof: See Appendix A.
The CRLB expression (21) explicitly reveals the impact of the lognormal shadowing variance σ_{ou}^2 of the UAV-GU link, of the path-loss exponent β, of the spatial correlation coefficient ρ and of the number of waypoints K on the lower bound. In particular, an increase in σ_{ou}^2 will result in a higher bound,

while the increase of β will lead to the reduction of the CRLB bound. Theoretical evaluations of the impact of ρ and K on CRB_i is challenge due to the complex of the CRLB expression. We present further discussions of this impact based on simulations in Section V. Additionally, the effect of the number of waypoints K on the CRLB under no shadowing correlation is characterized by the following corollary.

Corollary 1. *The inclusion of an additional waypoint reduces the CRLB.*

Proof: See Appendix B.
Remark: Note that (21) is for the scenario that the UAV's transmit power value P_u is updated at the GUs after the period of T (second) (denoted as *Scenario 1*). In cases that the GUs know the GS's transmit power value P_b but not P_u (denoted as *Scenario 2*), the noise term in (10) is a sum of two normally distributed variables, i.e., $\overline{S}_{uo,i}^{k[dB]} \triangleq S_{bu}^{[dB]} + S_{uo,i}^{k[dB]}$. In our system, we assume that the shadowing variables of the GS-UAV link and the UAV-GU link are independent. Thus, $\overline{S}_{uo,i}^{k[dB]}$ is a normal variable with variance of $\overline{\sigma}_{ou}^2 \triangleq \sigma_{ub}^2 + \sigma_{ou}^2$ (in dB). Additionally, it can be shown that the correlation coefficient between the RSS measurements becomes $\overline{\rho} = \frac{\sigma_{ub}^2 + \rho\sigma_{ou}^2}{\overline{\sigma}_{ou}^2}$ (see Appendix C). As a result, the CRLB expression in this case is obtained by replacing σ_{ou} and ρ in (21) by $\overline{\sigma}_{ou}$ and $\overline{\rho}$, respectively. Performance comparison between these two scenarios are provided in Section V.

IV. ANALYSIS OF OUTAGE PROBABILITY AND SYSTEM THROUGHPUT

We now consider the information transmission phase from the GUs to the GS. We analyze the OP and the TP both in delay-limited and delay-tolerant transmission modes. In our system, the DF relaying protocol is adopted at the UAV. Both the GU-UAV and UAV-GS links experience composite fading conditions of large-scale lognormal shadowing and small-scale Nakagami-m fading. Since the Nakagami-lognormal PDF has a more complex integral form, it is impossible to obtain closed-form expressions for the various system metrics. To circumvent this issue, we approximate the composite fading channels considered by using the mixture gamma (MG) distribution approach proposed in [39]. It is well established that a MG approximation can offer high accuracy for different kinds of fading channels. Thus, the results obtained in this work can be applied not only to other composite fading channels but also to small-scale fading channels, including $\eta - \mu$ channels and $\kappa - \mu$ channels, and Nakagami-q (*Hoyt*) channels. Since data transmission from the GUs to the GS is assumed to be performed on orthogonal subchannels, the index i is dropped throughout this section for simplicity.

A. Approximation of Fading Channel Distribution

We first describe some PDF approximations that will be utilized to facilitate derivations of closed-form expressions for both the OP and TP. For the lognormal shadowing, it is shown in [40] that the gamma PDF is capable of characterizing the

$$CRB_i \geq \frac{\sigma_{ou}\ln 10}{10\beta}\left(1 - \frac{(K-1)\rho^2}{(K-2)\rho+1}\right)^{1/2} \times$$

$$\left(\frac{\sum_{k=1}^{K}\left(X_{i,k}^2 + Y_{i,k}^2 - \frac{\rho}{(K-2)\rho+1}\sum_{\substack{n=1\\n\neq k}}^{K}(X_{i,k}X_{i,n} + Y_{i,k}Y_{i,n})\right)}{\sum_{k=1}^{K}\left(X_{i,k}^2 - \frac{\rho}{(K-2)\rho+1}\sum_{\substack{n=1\\n\neq k}}^{K}X_{i,k}X_{i,n}\right) \times \sum_{k=1}^{K}\left(Y_{i,k}^2 - \frac{\rho}{(K-2)\rho+1}\sum_{\substack{n=1\\n\neq k}}^{K}Y_{i,k}Y_{i,n}\right) - \left[\sum_{k=1}^{K}\left(X_{i,k}Y_{i,k} - \frac{\rho}{(K-2)\rho+1}\sum_{\substack{n=1\\n\neq k}}^{K}X_{i,k}Y_{i,n}\right)\right]^2}\right)^{1/2} \quad (21)$$

lognormal shadowing affects. In particular, the lognormal PDF that admits the form

$$f_{L,\phi}(x) = \frac{1}{\sqrt{2\pi\sigma_{L,\phi}^2}x}e^{-\frac{(\ln(x)-\mu_{L,\phi})^2}{2\sigma_{L,\phi}^2}}, \quad (22)$$

where $\mu_{L,\phi}$ and $\sigma_{L,\phi}$ represent the mean and the standard deviation, which can be approximated by the gamma PDF

$$f_{G,\phi}(x) = \frac{1}{\theta_\phi^{\varphi_\phi}\Gamma(\varphi_\phi)}x^{\varphi_\phi-1}e^{-x/\theta_\phi}, \quad (23)$$

where $\Gamma(.)$ is the gamma function and $\phi = \{ou, ub\}$ where *ou* stands for the channel between the GUs and the UAV, while *ub* is for the channel between the UAV and the GS. The relationship between the parameters of the gamma PDF and lognormal PDF is given by [40]

$$\sigma_{L,\phi} = \sqrt{\psi'(\varphi_\phi)}, \quad (24)$$

$$\mu_{L,\phi} = \ln(\theta_\phi) + \psi(\varphi_\phi), \quad (25)$$

where $\psi(.)$ and $\psi'(.)$ are the digamma (or Psi) and trigamma functions. The use of the gamma PDF is preferred to the lognormal PDF from an analytic computation perspective [40].

For the composite Nakagami-lognormal fading channel in either the GU-UAV or the UAV-GS link, the PDF can be expressed as

$$f_{NL,\phi}(x) = \int_0^\infty \frac{x^{m_\phi-1}e^{-m_\phi x/\varrho_\phi y}}{\Gamma(m_\phi)}\left(\frac{m_\phi}{\varrho_\phi y}\right)^{m_\phi}\frac{e^{-\frac{(\ln(y)-\mu_{L,\phi})^2}{2\sigma_{L,\phi}^2}}}{\sqrt{2\pi}\sigma_{L,\phi}y}dy, \quad (26)$$

where m_ϕ is the fading parameter of Nakagami-m fading and ϱ_ϕ is the unfaded SNR. By using a mixture gamma distribution approximation, we can approximate the above PDF by the following one [39]

$$f_{MG,\phi}(x) = \sum_{n=1}^{N_\phi}a_{\phi,n}x^{b_{\phi,n}-1}e^{-c_{\phi,n}x}, x \geq 0, \quad (27)$$

where N_ϕ is the number of terms, while $a_{\phi,n}$, $b_{\phi,n}$, and $c_{\phi,n}$ are the parameters associated with the nth Gamma component. These parameters are formulated as

$$a_{\phi,n} = \frac{\xi_n}{\sum_{j=1}^{N_\phi}\xi_j\Gamma(b_{\phi,j})c_{\phi,j}^{-b_{\phi,j}}},$$
$$b_{\phi,n} = m_\phi, \quad (28)$$
$$c_{\phi,n} = \frac{m_\phi}{\varrho_\phi}e^{-(\sqrt{2}\sigma_{L,\phi}\chi_n+\mu_{L,\phi})},$$

where $\xi_n = (m_\phi/\varrho_\phi)^{m_\phi}w_ne^{-m_\phi(\sqrt{2}\sigma_{L,\phi}\chi_n+\mu_{L,\phi})}/[\sqrt{\pi}\Gamma(m_\phi)]$, while χ_n and w_n are the abscissas and weight factors for the Gaussian-Hermite integration. Note that the accuracy of the MG approximation depends on the number of components N_ϕ, which is selected for ensuring that the mean-square error (MSE) between the lognormal-Nakagami-m distribution and the MG distribution is below a threshold. As shown in [39], the MSE accuracy requirement of 10^{-3} is guaranteed for $N_\phi = 8$. To achieve a better accuracy, a larger value of N_ϕ is needed.

From (27), the cumulative distribution function (CDF) of the MG distribution is

$$F_{MG,\phi}(x) = \sum_{n=1}^{N_\phi}a_{\phi,n}c_{\phi,n}^{-b_{\phi,n}}\gamma(b_{\phi,n}, c_{\phi,n}x), \quad (29)$$

where $\gamma(.,.)$ is the lower incomplete gamma function. Given the mathematically tractable form of the MG distribution, we can efficiently evaluate the system performance metrics of OP and TP in the next sections.

B. Outage Probability and Throughput in Delay-Limited Transmission

1) Outage probability: In our system model, outages are imposed by the composite fading in the GU-UAV and UAV-GS links. The OP is defined as the probability that the received SNR at the GS is below a given threshold. When DF-relaying is used by the UAV, it can be calculated as

$$P_{out}(\gamma_{th}) = Pr(\gamma_{ou} < \gamma_{th}) + Pr(\gamma_{ub} < \gamma_{th}, \gamma_{ou} \geq \gamma_{th}), \quad (30)$$

where γ_{th} is the SNR to be exceeded at the GS for correct data detection. The closed-form expression of P_{out} is formulated in the following theorem.

Theorem 2. *The OP of information transmission from a*

particular GU to the GS is given by

$$P_{out}(\gamma_{th}) =$$

$$\sum_{n=1}^{N_{ou}} a_{ou,n} c_{ou,n}^{-b_{ou,n}} \Gamma(b_{ou,n}) \left(1 - e^{-\frac{c_{ou,n}\gamma_{th}}{\overline{\gamma}_{ou}}} \sum_{m=0}^{b_{ou,n}-1} \frac{(c_{ou,n}\gamma_{th}/\overline{\gamma}_{ou})^m}{m!}\right)$$

$$+ \left[1 - \sum_{n=1}^{N_{ou}} a_{ou,n} c_{ou,n}^{-b_{ou,n}} \Gamma(b_{ou,n}) \left(1 - e^{-\frac{c_{ou,n}\gamma_{th}}{\overline{\gamma}_{ou}}} \times \right.\right.$$

$$\left.\left. \sum_{m=0}^{b_{ou,n}-1} \frac{(c_{ou,n}\gamma_{th}/\overline{\gamma}_{ou})^m}{m!} \right)\right] \times \sum_{n=1}^{N_{ub}} \left\{ a_{ub,n} c_{ub,n}^{-b_{ub,n}} \Gamma(b_{ub,n}) \left[1 - \right.\right.$$

$$\left.\left. \sum_{m=0}^{b_{ub,n}-1} \frac{2}{m!\Gamma(\varphi_{ub})} \left(\frac{c_{ub,n}\gamma_{th}}{\theta_{ub}\overline{\gamma}_{ub}}\right)^{\frac{\varphi_{ub}+m}{2}} K_{\varphi_{ub}-m}\left(2\sqrt{\frac{c_{ub,n}\gamma_{th}}{\theta_{ub}\overline{\gamma}_{ub}}}\right)\right]\right\}, \tag{31}$$

where $\overline{\gamma}_{ou} \triangleq \frac{P_o G_{ou}^1}{N_0}$, $\overline{\gamma}_{ub} \triangleq \frac{(K+2)(1-\alpha)\eta P_b G_{bu} G_{ub}}{(K+1)\alpha I N_0}$, and $K_\nu(.)$ is the ν-th order modified Bessel function of the second kind.

Proof: See Appendix D.1.

Note that the above expression consists of only elementary functions and the $K(.)$ function, hence it can be easily evaluated numerically. At high SNRs, we can derive an approximate OP expression provided by the following corollary.

Corollary 2. *The approximate OP in the high SNR regime is*

$$P_{out}(\gamma_{th}) \approx \sum_{n=1}^{N_{ou}} \frac{a_{ou,n}}{b_{ou,n}} \left(\frac{\gamma_{th}}{\overline{\gamma}_{ou}}\right)^{b_{ou,n}} + \left[1 - \sum_{n=1}^{N_{ou}} \frac{a_{ou,n}}{b_{ou,n}} \left(\frac{\gamma_{th}}{\overline{\gamma}_{ou}}\right)^{b_{ou,n}}\right]$$

$$\times \sum_{n=1}^{N_{ub}} a_{ub,n} c_{ub,n}^{-b_{ub,n}} \Gamma(b_{ub,n}) \left(1 - \sum_{m=0}^{b_{ub,n}-1} \frac{\Gamma(\varphi_{ub}-m)}{m!\Gamma(\varphi_{ub})} \times \right.$$

$$\left. \left(\frac{c_{ub,n}\gamma_{th}}{\theta_{ub}\overline{\gamma}_{ub}}\right)^m \left(1 - \frac{c_{ub,n}\gamma_{th}}{(\varphi_{ub}-m-1)\theta_{ub}\overline{\gamma}_{ub}}\right)\right). \tag{32}$$

Proof: See Appendix D.2.

2) Throughput in delay-limited transmission: In delay-limited (DL) scenarios, GUs transmit their data at a constant rate of R_c. For the whole block duration of T, the effective transmission time from a particular GU to the GS is $\alpha T/(K+2)$. The TP at the GS can be expressed as

$$\tau_{DL} = \frac{\alpha T/(K+2)}{T}(1-P_{out})R_c = \frac{\alpha}{K+2}(1-P_{out})R_c, \tag{33}$$

where P_{out} is the OP obtained in (31), and $R_c = \log_2(1 + \gamma_{th})$. Note that at high SNRs, we can obtain an approximate expression of the TP by substituting the result in (32) into (33). The total throughput of the whole system is the sum of the throughput of each user obtained in (33).

C. Throughput in Delay-Tolerant Transmission

For delay-tolerant (DT) scenarios, a source can transmit data at any rate upper-bounded by the ergodic capacity. Therefore, the TP can be obtained by evaluating the ergodic capacity. In particular, we have [17]

$$\tau_{DT} = \frac{\alpha T/(K+2)}{T}C = \frac{\alpha}{K+2}\min\{C_{ou}, C_{ub}\}, \tag{34}$$

where C is the ergodic capacity in a DF-relaying protocol, i.e., $C = \min\{C_{ou}, C_{ub}\}$ where C_{ou} and C_{ub} are the ergodic capacities of the GU-UAV link and the UAV-GS link, respectively. These capacities are given by

$$C_{ou} = \mathbb{E}\{\log_2(1 + \gamma_{ou})\}, \tag{35}$$

and

$$C_{ub} = \mathbb{E}\{\log_2(1 + \gamma_{ub})\}. \tag{36}$$

By performing some further mathematical manipulations, we obtain the closed-form expressions of C_{ou} and C_{ub} in the following theorem.

Theorem 3. *The ergodic capacities of the GU-UAV and UAV-GS links are given by*

$$C_{ou} = \frac{1}{\ln 2} \sum_{n=1}^{N_{ou}} a_{ou,n} c_{ou,n}^{-b_{ou,n}} \Gamma(b_{ou,n}) \left(\frac{c_{ou,n}}{\overline{\gamma}_{ou}}\right)^{b_{ou,n}} \times$$

$$e^{\frac{c_{ou,n}}{\overline{\gamma}_{ou}}} \sum_{v=1}^{b_{ou,n}} \frac{\Gamma(-b_{ou,n}+v, c_{ou,n}/\overline{\gamma}_{ou})}{(c_{ou,n}/\overline{\gamma}_{ou})^v}, \tag{37}$$

and

$$C_{ub} = \frac{1}{\ln 2} \sum_{n=1}^{N_{ub}} a_{ub,n} c_{ub,n}^{-b_{ub,n}} (b_{ub,n}-1)! \sum_{m=0}^{b_{ub,n}-1} \frac{1}{m!\Gamma(\varphi_{ub})} \times$$

$$\left[-m G_{4,2}^{1,4}\left(\frac{\theta_{ub}\overline{\gamma}_{ub}}{c_{ub,n}}\middle| \begin{array}{c} -\varphi_{ub}+1, -m+1, 1, 1 \\ 1, 0 \end{array}\right) + \right.$$

$$\left. G_{4,2}^{1,4}\left(\frac{\theta_{ub}\overline{\gamma}_{ub}}{c_{ub,n}}\middle| \begin{array}{c} -\varphi_{ub}+1, -m, 1, 1 \\ 1, 0 \end{array}\right)\right], \tag{38}$$

where $\Gamma(.,.)$ and $G_{p,q}^{m,n}(.)$ are the upper incomplete gamma function and the Meijer G-function, respectively.

Proof: See Appendix E.1.

It is worth mentioning that the Meijer G-function is a standard built-in function in several software packages, such as Matlab or Mathematica. Hence, the system throughput can be evaluated efficiently based on the expressions derived. Additionally, in the high SNR regime, a simpler approximate expression can be obtained for the ergodic capacities by utilizing the approximation of $\log(1 + x) \approx \log(x)$, when $x \to \infty$.

Corollary 3. *The approximate ergodic capacities under delay-tolerant scenarios in the high SNR regime are given by*

$$C_{ou} \approx \frac{1}{\ln 2} \sum_{n=1}^{N_{ou}} a_{ou,n} c_{ou,n}^{-b_{ou,n}} \Gamma(b_{ou,n}) \left[\psi(b_{ou,n}) - \ln\left(\frac{c_{ou,n}}{\overline{\gamma}_{ou}}\right)\right] \tag{39}$$

and

$$C_{ub} \approx \frac{1}{\ln 2} \sum_{n=1}^{N_{ub}} a_{ub,n} c_{ub,n}^{-b_{ub,n}} \Gamma(b_{ub,n}) \times$$

$$\left[\psi(\varphi_{ub}+1) + \psi(1) - \ln\left(\frac{c_{ub,n}}{\theta_{ub}\overline{\gamma}_{ub}}\right) + \sum_{m=1}^{b_{ub,n}-1} \frac{1}{m}\right], \tag{40}$$

where $\psi(.)$ is the Psi function [33, Eq. (8.360.1)].

Proof: See Appendix E.2.

D. Optimal Energy-Harvesting Time for Maximal Throughput

In the previous sections, the expressions of the achievable throughput of both the delay-tolerant and delay-limited transmission modes have been derived. We now examine the optimal energy-harvesting time fraction α^{opt} designed for maximal throughput. The high SNR region is considered for the analytical results. In a delay-limited transmission mode, it is an open challenge to derive a closed-form expression for α^{opt}. For a delay-tolerant mode, the result is given by the following theorem.

Theorem 4. *The optimal energy-harvesting time fraction for the maximal throughput under delay-tolerant transmissions in the high SNR regime is*

$$\alpha^{opt} = \frac{1}{1 + e^{W(e^{\Phi/\Upsilon - 1}) + 1 - \Phi/\Upsilon}}, \quad (41)$$

where $W(.)$ is the Lambert W function [41],

$$\Phi \triangleq \frac{1}{\ln 2} \sum_{n=1}^{N_{ub}} a_{ub,n} c_{ub,n}^{-b_{ub,n}} \Gamma(b_{ub,n}) \Bigg[\psi(\varphi_{ub} + 1) + \psi(1) +$$

$$\ln\left(\frac{\theta_{ub}(K+2)\eta P_b G_{bu} G_{ub}}{c_{ub,n}(K+1) I N_0}\right) + \sum_{m=1}^{b_{ub,n}-1} \frac{1}{m}\Bigg], \quad (42)$$

and

$$\Upsilon \triangleq \frac{1}{\ln 2} \sum_{n=1}^{N_{ub}} a_{ub,n} c_{ub,n}^{-b_{ub,n}} \Gamma(b_{ub,n}). \quad (43)$$

Proof: See Appendix F.
Simulations matching these results are provided in Section V.

V. SIMULATION RESULTS AND DISCUSSIONS

In this section, we provide simulation results for validating the analysis of the previous sections. We assume that $I = 100$ GUs are uniformly distributed in an area of $100m \times 100m$, centered at (0,0), while the GS is located at a position of $(150m, 0)$. The UAV flies at the height of $h(m)$ through K waypoints that is specified by a circle with a radius of $R(m)$. Specifically, the position of the kth waypoint is (x_k, y_k, h), where $x_k = R \cos \frac{2\pi(k-1)}{K}$ and $y_k = R \sin \frac{2\pi(k-1)}{K}, k = 1, 2, ..., K$. The simulation results are evaluated by using the actual lognormal-Nakagami-*m* fading channel coefficients, while the analysis results are obtained based on the MG distribution approximation described in Section IV. To generate correlated shadowing coefficients, we use the Cholesky decomposition for decomposing the covariance matrix Λ_i. In particular, we have $\Lambda_i = \Delta\Delta^T$, where Δ is a lower triangular matrix. Thus, the vector of shadowing components S_i associated with the covariance matrix of Λ_i is generated as $S_i = \Lambda_i n$, where n is a vector of zero-mean, unit-variance i.i.d. Gaussian random variables [10]. Unless otherwise specified, the other parameters are used in our simulations are: $h = 50(m), R = 30(m), \beta = 2, g_0 = -30$ (dB), $\eta = 0.8$, $\alpha = 0.7, m_\phi = 2, N_\phi = 8, \rho = 0.4, \sigma_{ou} = \sigma_{ub} = 1$ (dB), $P_b = 10$ W, $P_{o,i} = 100$ mW, $R_c = 1 (bps/Hz)$ and $N_0 = 10^{-15}$ W. The results are averaged over 10^3 channel realizations.
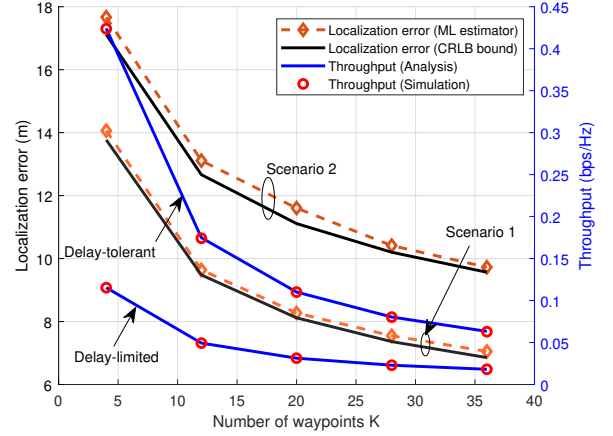

Fig. 3: Localization error and throughput versus the number of waypoints K.

A. Impact of the Number of Waypoints and the UAV Altitude

We first investigate the impact of the number of waypoints as well as of the UAV altitude on both the localization error and the throughput. In Figure 3, we plot the localization error in terms of the root mean-square error (RMSE) together with the throughput versus the number of waypoints K. It can be readily seen that the error is reduced when K increases, which indicates the significant impact of adding more waypoints on the localization accuracy. This also agrees our analysis result in Corollary 1. As expected, the localization error attained in *Scenario 1*, where the UAV's transmit power value P_u is known, is smaller than that in *Scenario 2* where the value P_u is unknown by the GUs. From a mathematical viewpoint, the performance degradation in *Scenario 2* is mainly because the equivalent noise variance $\overline{\sigma}_{ou}^2$ is higher than σ_{ou}^2 in *Scenario 1* (cf.(21)). Note that the advantage in *Scenario 1* comes at the cost of the inclusion of the value P_u in the UAV broadcast signals. Additionally, the average running time of the ML estimator on CPU AMD Athlon Silver 3050U 2.3 GHz with the numbers of waypoints set to $K = 4, 12, 20, 28$, and 36 are $5.7(ms), 6.2(ms), 7.7(ms), 9.7(ms)$, and $12.3(ms)$, respectively. Regarding the throughput, Figure 3 illustrates that the achievable throughput is reduced, when K increases. This is because the time period allocated for information transmission will be reduced when K increases. Thus there exists a compromise between the localization error at the GUs and the throughput at the GS. Note that the analytical results match well with the simulation, which confirms the tightness of the derived bound as well as the accuracy of the expressions derived in Section IV.

Figure 4 shows both the localization error and throughput versus the UAV altitude. It can be seen that the UAV's altitude has a significant influence on the localization error. Specifically, the localization error increases upon increasing the altitude h. When h becomes large, the distance between the UAV and the GUs is very large. Therefore, the localization error becomes larger (cf. (21)). With respect to the system throughput, the result shows that its value decreases when h increases. This is due to the fact that the longer transmission distance results in reduced capacities and increased OP.
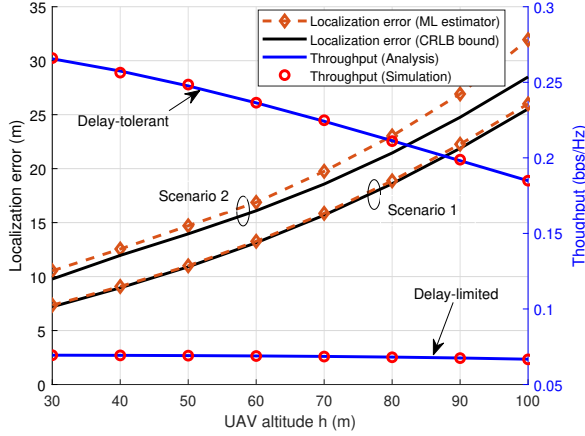
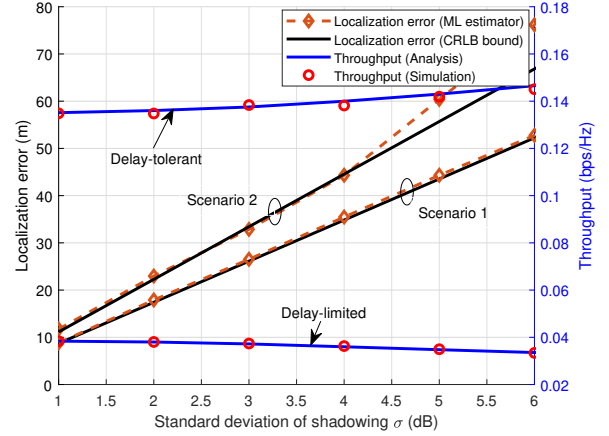Fig. 4: Localization error and throughput versus the UAV altitude ($K = 8$).

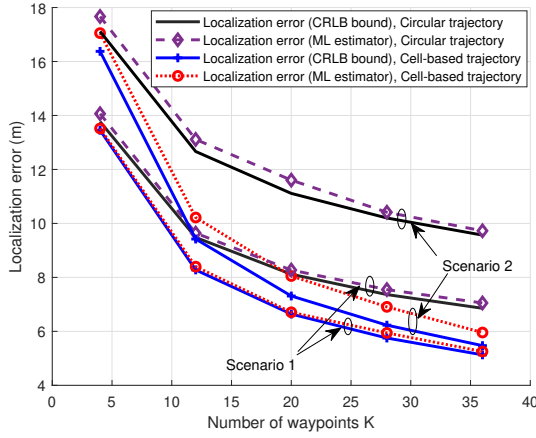Fig. 5: Localization error versus the number of waypoints under different trajectories.

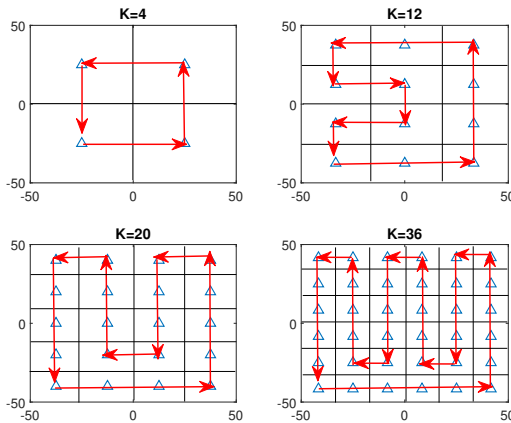Fig. 6: An illustration of the cell-based trajectory ($\triangle$ denotes a waypoint).

Given a specific number of waypoints K and UAV altitude h, the localization performance also depends on the positions of the waypoints themselves. To demonstrate this, we plot in Fig. 5 the localization errors for two different trajectories, namely the circular trajectory as mentioned earlier and a cell-

Fig. 7: Localization error and throughput versus the shadowing standard deviation ($K = 16$).

based trajectory, as illustrated in Fig. 6. For the cell-based trajectory, the whole area is divided into equal cells, and the waypoints are at the centre of the cells. It can be seen from Fig. 5 that the UAV associated with the cell-based trajectory could achieve a higher localization accuracy than its counterpart. Note that this comparison does not take into considerations the length of the trajectory, which is constrained by many factors, including the time required to accomplish the localization task, the energy budget of the UAV, or geographical conditions. Additionally, the optimality of UAV trajectory might be affected by the distribution of the GUs. Having said that the optimal trajectory design is beyond the scope of this treatise, the readers are referred to [28], [30]-[32], and [42] for design approaches.

B. Impact of Fading Parameters

We next evaluate the impact of the fading environment, including the shadowing variances, the spatial correlation of shadowing and the small-scale Nakagami-m fading parameter. In particular, Figure 7 shows the localization error and throughput versus the standard deviation of the lognormal shadowing. It can be seen that the localization error increases upon increasing the shadowing. As for the system throughput, it is interesting to note that when σ is larger, the throughput achieved in the delay-limited mode becomes lower, whereas in the delay-tolerant mode it is higher. This behavior of the ergodic capacity (and thus the throughput) under composite fading channels was reported in the literature [43].

In Figure 8a, we plot the localization error versus the shadowing correlation coefficient ρ, which shows that the error is reduced when ρ increases. The impact of the shadowing correlation is similar that in [10], where four anchor nodes were deployed. Additionally, Figure 8b demonstrates that the system throughput is enhanced when m increases, representing better small-scale fading conditions.

C. Impact of Energy-Harvesting Time on Throughput

Finally, we examine the optimal energy-harvesting time in the system. Figure 9a shows the achievable throughput versus
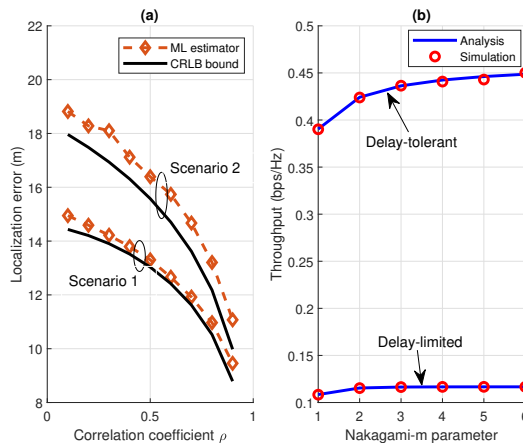
Fig. 8: (a) Localization error versus shadowing correlation coefficient; (b) Throughput versus Nakagami-m parameter ($K = 4$).
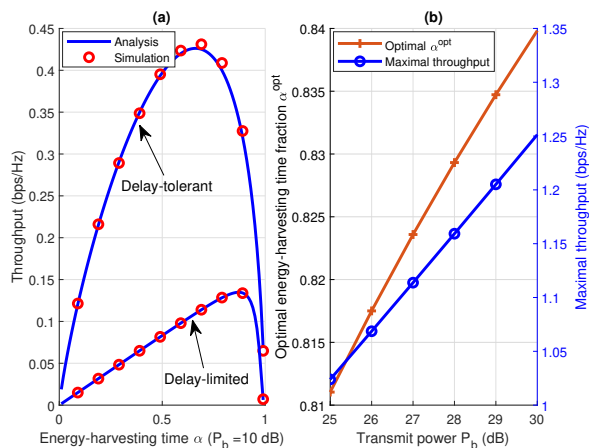

Fig. 9: (a) Throughput versus energy-harvesting time; (b) Optimal energy-harvesting time and maximal throughput versus transmit power P_b ($K = 4$).

the energy-harvesting time fraction α. Firstly, it can be seen that the throughput first increases then decreases when α increases for both the delay-limited and delay-tolerant modes. This behavior is characterized by the trade-offs between the time period used for harvesting energy and the OP (for delay-limited) or ergodic capacity (for delay-tolerant). This trade-off is also observed in other energy-harvesting based relaying systems [17], [18]. Secondly, there exists an optimal energy-harvesting time fraction attaining the maximal throughput. The optimal value α^{opt} versus the value P_b is shown in Figure 9b. It can be seen that α^{opt} is increased, when P_b increases. This behavior can be evaluated from the analytical result of (41). Figure 9b also shows that the maximal throughput is improved, when the GS's transmit power is increased.

VI. CONCLUSIONS

We have harnessed energy-harvesting aided UAVs for terrestrial localization systems subjected to lognormal-Nakagami-m fading channels. The performance of RSS-based localization at the GUs in spatially correlated shadowing environments has been examined via the CRLB derived. The system has

been analyzed in terms of its OP, egordic capacity and achievable throughput. The results unveil the significant impact of the number of waypoints and the UAV altitude, of the spatial correlation level and fading parameters, as well as of the energy-harvesting time fraction on both localization and communications. These results facilitate an exploration of different trade-offs and provide useful insights into the system design. Our future research would include investigating optimal UAV trajectory designs using a machine learning approach, taking into account the practical requirements of the UAV's propulsion mechanisms, and combining the RSS-based method with other localization methods, such as TOA and AOA, for attaining a further improved system performance.

APPENDIX A
CALCULATION OF THE ELEMENTS OF FISHER INFORMATION MATRIX (FIM)

The entries of the FIM defined in (19) is calculated as [38]

$$F_{\mathrm{uv}}(\mathcal{L}_i) = \frac{\partial \boldsymbol{\Theta}_i^T}{\partial \mathrm{u}} \boldsymbol{\Lambda}_i^{-1} \frac{\partial \boldsymbol{\Theta}_i}{\partial \mathrm{v}} + \frac{1}{2} tr \left\{ \boldsymbol{\Lambda}_i^{-1} \frac{\partial \boldsymbol{\Lambda}_i}{\partial \mathrm{u}} \boldsymbol{\Lambda}_i^{-1} \frac{\partial \boldsymbol{\Lambda}_i}{\partial \mathrm{v}} \right\}, (44)$$

where $\mathrm{u}, \mathrm{v} \in \{x_i, y_i\}$, $tr\{.\}$ denotes the trace of a matrix, $\boldsymbol{\Theta}_i$ is the mean vector and

$$\frac{\partial \boldsymbol{\Theta}_i^T}{\partial \mathrm{u}} = \left[\frac{\partial [\boldsymbol{\Theta}_i]_1}{\partial \mathrm{u}}, \frac{\partial [\boldsymbol{\Theta}_i]_2}{\partial \mathrm{u}}, ..., \frac{\partial [\boldsymbol{\Theta}_i]_K}{\partial \mathrm{u}} \right], \quad (45)$$

In our system model, $\boldsymbol{\Lambda}_i$ is independent of $\mathcal{L}_i$. Thus, (44) can be simplified to

$$F_{\mathrm{uv}}(\mathcal{L}_i) = \frac{\partial \boldsymbol{\Theta}_i^T}{\partial \mathrm{u}} \boldsymbol{\Lambda}_i^{-1} \frac{\partial \boldsymbol{\Theta}_i}{\partial \mathrm{v}}. \quad (46)$$

From (45), (46), and (12), we have

$$F_{\mathrm{uv}}(\mathcal{L}_i) = \frac{1}{[1 + (K-2)\rho - (K-1)\rho^2]\sigma_{ou}^2} \times$$
$$\sum_{k=1}^{K} \left([(K-2)\rho + 1] \frac{\partial [\boldsymbol{\Theta}_i]_k}{\partial \mathrm{u}} \frac{\partial [\boldsymbol{\Theta}_i]_k}{\partial \mathrm{v}} - \rho \sum_{n=1, n \neq k}^{K} \frac{\partial [\boldsymbol{\Theta}_i]_k}{\partial \mathrm{u}} \frac{\partial [\boldsymbol{\Theta}_i]_n}{\partial \mathrm{v}} \right). \quad (47)$$

Note that $\frac{\partial [\boldsymbol{\Theta}_i]_k}{\partial x_i} = -\frac{10\beta(x_i - \mathrm{x}_k)}{d_{i,n}^2 \ln 10}$ and $\frac{\partial [\boldsymbol{\Theta}_i]_k}{\partial y_i} = -\frac{10\beta(y_i - \mathrm{y}_k)}{d_{i,n}^2 \ln 10}$. By substituting these results into (47), we have

$$F_{x_i x_i}(\mathcal{L}_i) = \frac{1}{1 + (K-2)\rho - [(K-1)\rho^2]\sigma_{ou}^2} \times \left(\frac{10\beta}{\ln 10} \right)^2 \times$$
$$\sum_{k=1}^{K} \left([(K-2)\rho + 1] \frac{(x_i - \mathrm{x}_k)^2}{d_{i,k}^4} - \rho \sum_{n=1, n \neq k}^{K} \frac{(x_i - \mathrm{x}_k)(x_i - \mathrm{x}_n)}{d_{i,k}^2 d_{i,n}^2} \right), (48)$$

$$F_{y_i y_i}(\mathcal{L}_i) = \frac{1}{1+(K-2)\rho-[(K-1)\rho^2]\sigma_{ou}^2} \times \left(\frac{10\beta}{\ln 10}\right)^2 \times$$

$$\sum_{k=1}^{K}\left([(K-2)\rho+1]\frac{(y_i-\mathrm{y}_k)^2}{d_{i,k}^4} - \rho\sum_{n=1,n\neq k}^{K}\frac{(y_i-\mathrm{y}_k)(y_i-\mathrm{y}_n)}{d_{i,k}^2 d_{i,n}^2}\right), \quad (49)$$

$$F_{x_i y_i}(\mathcal{L}_i) = F_{y_i x_i}(\mathcal{L}_i) =$$

$$\frac{1}{1+(K-2)\rho-[(K-1)\rho^2]\sigma_{ou}^2} \times \left(\frac{10\beta}{\ln 10}\right)^2 \times$$

$$\sum_{k=1}^{K}\left([(K-2)\rho+1]\frac{(x_i-\mathrm{x}_k)(y_i-\mathrm{y}_k)}{d_{i,k}^4} - \rho\sum_{n=1,n\neq k}^{K}\frac{(x_i-\mathrm{x}_k)(y_i-\mathrm{y}_n)}{d_{i,k}^2 d_{i,n}^2}\right). \quad (50)$$

Note that $\sum_{k=1}^{K}\sum_{n=1,n\neq k}^{K}\frac{(x_i-\mathrm{x}_k)(y_i-\mathrm{y}_n)}{d_{i,k}^2 d_{i,n}^2} = \sum_{k=1}^{K}\sum_{n=1,n\neq k}^{K}\frac{(y_i-\mathrm{y}_k)(x_i-\mathrm{x}_n)}{d_{i,k}^2 d_{i,n}^2}$, thus we have $F_{x_i y_i}(\mathcal{L}_i) = F_{y_i x_i}(\mathcal{L}_i)$. Finally, (21) is obtained by substituting the above results into (20).

APPENDIX B
PROOF OF COROLLARY 1

When $\rho = 0$, the CRLB in (21) is simplified to $CRB_i = \frac{\sigma_{ou}\ln 10}{10\beta}\sqrt{g(K)}$, where

$$g(K) \triangleq \frac{\sum_{k=1}^{K}(X_{i,k}^2 + Y_{i,k}^2)}{\sum_{k_1=1}^{K}\sum_{k_2=1}^{K}(X_{i,k_1}^2 Y_{i,k_2}^2 - X_{i,k_1}X_{i,k_2}Y_{i,k_1}Y_{i,k_2})} \quad (51)$$

To show that CRB_i is a decreasing function, we prove that $g(K)$ decreases, when K increases. In other words, we will show that $g(K) - g(K+1) \geq 0$. From (51), we can express

$$g(K) - g(K+1) = \frac{\mathcal{U}(K)}{\mathcal{V}(K)}, \quad (52)$$

where

$$\mathcal{U}(K) \triangleq$$
$$\left(\sum_{k=1}^{K}(X_k^2 + Y_k^2)\right)\left(\sum_{k_1=1}^{K+1}\sum_{k_2=1}^{K+1}(X_{k_1}^2 Y_{k_2}^2 - X_{k_1}X_{k_2}Y_{k_1}Y_{k_2})\right) -$$
$$\left(\sum_{k=1}^{K+1}(X_k^2+Y_k^2)\right)\left(\sum_{k_1=1}^{K}\sum_{k_2=1}^{K}(X_{k_1}^2 Y_{k_2}^2 - X_{k_1}X_{k_2}Y_{k_1}Y_{k_2})\right), \quad (53)$$

and

$$\mathcal{V}(K) \triangleq \left(\sum_{k_1=1}^{K}\sum_{k_2=1}^{K}(X_{k_1}^2 Y_{k_2}^2 - X_{k_1}X_{k_2}Y_{k_1}Y_{k_2})\right) \times$$
$$\left(\sum_{k_1=1}^{K+1}\sum_{k_2=1}^{K+1}(X_{k_1}^2 Y_{k_2}^2 - X_{k_1}X_{k_2}Y_{k_1}Y_{k_2})\right). \quad (54)$$

In what follows, we will prove that both the denominator and numerator of (52) are non-negative. Let us first consider the denominator. To show that $\mathcal{V}(K) \geq 0$, we have to show that

$$\mathcal{W}(K) \triangleq \sum_{k_1=1}^{K}\sum_{k_2=1}^{K}(X_{k_1}^2 Y_{k_2}^2 - X_{k_1}X_{k_2}Y_{k_1}Y_{k_2}) \geq 0, \forall K \geq 1 \quad (55)$$

We use the mathematical induction proof. To start with, when $K = 1$, (55) is reduced to

$$\mathcal{W}(1) = X_1^2 Y_1^2 - X_1 X_1 Y_1 Y_1 = 0. \quad (56)$$

When $K = 2$, (55) is reduced to

$$\mathcal{W}(2) = \sum_{k_1=1}^{2}\sum_{k_2=1}^{2}(X_{k_1}^2 Y_{k_2}^2 - X_{k_1}X_{k_2}Y_{k_1}Y_{k_2})$$
$$= (X_1 Y_2 - X_2 Y_1)^2 \geq 0. \quad (57)$$

Now, assuming that (55) holds for K, i.e., $\mathcal{W}(K) \geq 0$, we will show that $\mathcal{W}(K+1) \geq 0$. Indeed, we can write that

$$\mathcal{W}(K+1) = \sum_{k_1=1}^{K+1}\sum_{k_2=1}^{K+1}(X_{k_1}^2 Y_{k_2}^2 - X_{k_1}X_{k_2}Y_{k_1}Y_{k_2})$$
$$= \mathcal{W}(K) + X_{K+1}^2\sum_{k_2=1}^{K}Y_{k_2}^2 - X_{K+1}Y_{K+1}\sum_{k_2=1}^{K}X_{k_2}Y_{k_2} +$$
$$Y_{K+1}^2\sum_{k_1=1}^{K}X_{k_1}^2 - X_{K+1}Y_{K+1}\sum_{k_1=1}^{K}X_{k_1}Y_{k_1} +$$
$$X_{K+1}^2 Y_{K+1}^2 - X_{K+1}Y_{K+1}X_{K+1}Y_{K+1}$$
$$= \mathcal{W}(K) + \sum_{k=1}^{K}(X_{K+1}Y_k - X_k Y_{K+1})^2. \quad (58)$$

It is plausible that $\mathcal{W}(K+1) \geq 0$ given that $\mathcal{W}(K) \geq 0$. Therefore, we have $\mathcal{V}(K) \geq 0, \forall K \geq 1$.

Next, we show that the numerator $\mathcal{U}(K) \geq 0, \forall K \geq 1$. By using the result in (58) and noting that $\sum_{k_1=1}^{K}\sum_{k_2=1}^{K}(X_{k_1}^2 Y_{k_2}^2 - X_{k_1}X_{k_2}Y_{k_1}Y_{k_2}) = \sum_{k=1}^{K}X_k^2\sum_{k=1}^{K}Y_k^2 - \left(\sum_{k=1}^{K}X_k Y_k\right)^2$, we can rewrite (53) as

$$\mathcal{U}(K) = \left(\sum_{k=1}^{K}(X_k^2 + Y_k^2)\right) \times \left(\sum_{k=1}^{K}(X_{K+1}Y_k - X_k Y_{K+1})^2\right)$$
$$- \left(X_{K+1}^2 + Y_{K+1}^2\right) \times \left(\sum_{k=1}^{K}X_k^2\sum_{k=1}^{K}Y_k^2 - \left(\sum_{k=1}^{K}X_k Y_k\right)^2\right)$$
$$= X_{K+1}^2\left[\left(\sum_{k=1}^{K}X_k^2 + \sum_{k=1}^{K}Y_k^2\right)\sum_{k=1}^{K}Y_k^2 - \sum_{k=1}^{K}X_k^2\sum_{k=1}^{K}Y_k^2 + \left(\sum_{k=1}^{K}X_k Y_k\right)^2\right] + Y_{K+1}^2\left[\left(\sum_{k=1}^{K}X_k^2 + \sum_{k=1}^{K}Y_k^2\right)\sum_{k=1}^{K}X_k^2 - \sum_{k=1}^{K}X_k^2\sum_{k=1}^{K}Y_k^2 + \left(\sum_{k=1}^{K}X_k Y_k\right)^2\right] -$$
$$2X_{K+1}Y_{K+1}\left(\sum_{k=1}^{K}X_k^2 + \sum_{k=1}^{K}Y_k^2\right)\sum_{k=1}^{K}X_k Y_k. \quad (59)$$

After some further manipulations, we obtain

$$\mathcal{U}(K) = \left(X_{K+1}\sum_{k=1}^{K}Y_k^2 - Y_{K+1}\sum_{k=1}^{K}X_k Y_k\right)^2 +$$
$$\left(Y_{K+1}\sum_{k=1}^{K}X_k^2 - X_{K+1}\sum_{k=1}^{K}X_k Y_k\right)^2 \geq 0. \quad (60)$$

The proof is thus completed.

APPENDIX C
CALCULATION OF CORRELATION COEFFICIENTS

In *Scenario 2*, the shadowing associated with the location estimation of the ith GU is characterized by $\overline{S}_{uo,i}^{k[dB]} = S_{bu}^{[dB]} + S_{uo,i}^{k[dB]}, k = 1, 2, ..., K$, where $S_{bu}^{[dB]} \in \mathcal{CN}(0, \sigma_{ub}^2)$ and $S_{uo,i}^{k[dB]} \in \mathcal{CN}(0, \sigma_{ou}^2)$. Thus, the covariance matrix of the RSS measurements at the ith GU is given by

$$cov\left(\overline{\mathbf{S}}_{uo,i}^{[dB]}\right) = cov\left(\mathbf{S}_{bu}^{[dB]} + \mathbf{S}_{uo,i}^{[dB]}\right), \qquad (61)$$

where $\overline{\mathbf{S}}_{uo,i}^{[dB]} \triangleq [\overline{S}_{uo,i}^{1[dB]}, \overline{S}_{uo,i}^{2[dB]}, ..., \overline{S}_{uo,i}^{K[dB]}]$, $\mathbf{S}_{bu}^{[dB]} \triangleq [S_{bu}^{[dB]}, S_{bu}^{[dB]}, ..., S_{bu}^{[dB]}]$ and $\mathbf{S}_{uo,i}^{[dB]} \triangleq [S_{uo,i}^{1[dB]}, S_{uo,i}^{2[dB]}, ..., S_{uo,i}^{K[dB]}]$. The (m, n) entry of this covariance matrix can be formulated as [44]

$$cov\left(\overline{S}_{uo,i}^{m[dB]}, \overline{S}_{uo,i}^{n[dB]}\right) = cov\left(S_{bu}^{[dB]} + S_{uo,i}^{m[dB]}, S_{bu}^{[dB]} + S_{uo,i}^{n[dB]}\right)$$
$$= cov\left(S_{bu}^{[dB]}, S_{bu}^{[dB]}\right) + cov\left(S_{bu}^{[dB]}, S_{uo,i}^{n[dB]}\right)$$
$$+ cov\left(S_{uo,i}^{m[dB]}, S_{bu}^{[dB]}\right) + cov\left(S_{uo,i}^{m[dB]}, S_{uo,i}^{n[dB]}\right). \qquad (62)$$

Since the shadowing variables $S_{bu}^{[dB]}$ and $S_{uo,i}^{n[dB]}$ are independent, we have $cov\left(S_{bu}^{[dB]}, S_{uo,i}^{n[dB]}\right) = 0, \forall n$. Recall that $cov\left(S_{uo,i}^{m[dB]}, S_{uo,i}^{n[dB]}\right) = \sigma_{ou}^2 \rho_{m,n}$. Thus, (62) is simplified to

$$cov\left(\overline{S}_{uo,i}^{m[dB]}, \overline{S}_{uo,i}^{n[dB]}\right) = cov\left(S_{bu}^{[dB]}, S_{bu}^{[dB]}\right) + \sigma_{ou}^2 \rho_{m,n}$$
$$= \sigma_{ub}^2 + \sigma_{ou}^2 \rho_{m,n}. \qquad (63)$$

Finally, the correlation coefficient associated with the (m, n) entry of the covariance matrix is obtained as [44]

$$\overline{\rho}_{m,n} = \frac{cov\left(\overline{S}_{uo,i}^{m[dB]}, \overline{S}_{uo,i}^{n[dB]}\right)}{\sqrt{var\left(\overline{S}_{uo,i}^{m[dB]}\right)}\sqrt{var\left(\overline{S}_{uo,i}^{n[dB]}\right)}} = \frac{\sigma_{ub}^2 + \sigma_{ou}^2 \rho_{m,n}}{\overline{\sigma}_{ou}^2},$$

$$(64)$$

where $\overline{\sigma}_{ou}^2 \triangleq \sigma_{ub}^2 + \sigma_{ou}^2$. This completes the proof.

APPENDIX D
DERIVATION OF OUTAGE PROBABILITY

1) Exact expression of outage probability: The first term in (30), which is the outage probability at the UAV, can be calculated as (cf. (6))

$$Pr(\gamma_{ou} < \gamma_{th}) = Pr\left(\frac{P_o G_{ou}^1 S_{ou}^1 H_{ou}^1}{N_0} < \gamma_{th}\right)$$
$$= Pr\left(S_{ou}^1 H_{ou}^1 < \frac{\gamma_{th} N_0}{P_o G_{ou}^1}\right) = F_{\mathcal{M}_{ou}^1}\left(\frac{\gamma_{th} N_0}{P_o G_{ou}^1}\right), \quad (65)$$

where $\mathcal{M}_{ou}^1 \triangleq S_{ou}^1 H_{ou}^1$ and $F_{\mathcal{M}_{ou}^1}(x)$ is the CDF of $\mathcal{M}_{ou}^1$. We note that the composite fading $\mathcal{M}_{ou}^1$ of the GU-UAV link follows the lognormal-Nakagami-m distribution. Thus, its CDF can be expressed by using the mixture gamma approach, as shown in Section IV.A. Specifically, (65) can be expressed as (cf. (29))

$$Pr(\gamma_{ou} < \gamma_{th}) = \sum_{n=1}^{N_{ou}} a_{ou,n} c_{ou,n}^{-b_{ou,n}} \gamma\left(b_{ou,n}, \frac{\gamma_{th} N_0}{P_o G_{ou}^1} c_{ou,n}\right), \quad (66)$$

where the parameters $N_{ou}, a_{ou,n}, b_{ou,n}$, and $c_{ou,n}$ are defined as in (28). In this work, we consider integer values of the Nakagami fading paramter m. Thus, $b_{ou,n}$ is a positive integer number (cf. (28)). By using the result in [33, Eq. (8.352.1)], we can rewrite (66) as

$$Pr(\gamma_{ou} < \gamma_{th}) = \sum_{n=1}^{N_{ou}} a_{ou,n} c_{ou,n}^{-b_{ou,n}} \Gamma(b_{ou,n}) \times$$
$$\left[1 - e^{-\frac{c_{ou,n}\gamma_{th}}{\overline{\gamma}_{ou}}} \sum_{m=0}^{b_{ou,n}-1} \frac{(c_{ou,n}\gamma_{th}/\overline{\gamma}_{ou})^m}{m!}\right], \quad (67)$$

where $\overline{\gamma}_{ou} \triangleq \frac{P_o G_{ou}^1}{N_0}$.

The second term in (30), which accounts for the outage probability at the GS given that no outage occurs at the UAV, can be formulated as

$$Pr(\gamma_{ub} < \gamma_{th}, \gamma_{ou} \geq \gamma_{th}) = Pr(\gamma_{ub} < \gamma_{th})Pr(\gamma_{ou} \geq \gamma_{th})$$
$$= Pr(\gamma_{ub} < \gamma_{th})\left[1 - Pr(\gamma_{ou} < \gamma_{th})\right]. \quad (68)$$

Note that the above result is obtained, since γ_{ub} and γ_{ou} are independent. The probability $Pr(\gamma_{ub} < \gamma_{th})$ can be expressed as (cf. (7))

$$Pr(\gamma_{ub} < \gamma_{th})$$
$$= Pr\left(\frac{(K+2)(1-\alpha)\eta P_b G_{bu} G_{ub} S_{bu} S_{ub} H_{ub}}{(K+1)\alpha I N_0} < \gamma_{th}\right)$$
$$= Pr\left(S_{bu} S_{ub} H_{ub} < \frac{(K+1)\alpha I N_0 \gamma_{th}}{(K+2)(1-\alpha)\eta P_b G_{bu} G_{ub}}\right)$$
$$= Pr\left(S_{bu} \times \mathcal{M}_{ub} < \gamma_{th}/\overline{\gamma}_{ub}\right), \quad (69)$$

where $\mathcal{M}_{ub} \triangleq S_{ub} H_{ub}$ and $\overline{\gamma}_{ub} \triangleq \frac{(K+2)(1-\alpha)\eta P_b G_{bu} G_{ub}}{(K+1)\alpha I N_0}$. Recall that S_{bu} and $\mathcal{M}_{ub}$ are the lognormal and Nakagami-lognormal random variables, respectively. By using the approximation results in Section IV.A, we have

$$Pr(\gamma_{ub} < \gamma_{th}) = Pr\left(\mathcal{M}_{ub} < \frac{\gamma_{th}}{\overline{\gamma}_{ub} S_{bu}}\right)$$
$$= \int_0^{+\infty} F_{\mathcal{M}_{ub}}\left(\frac{\gamma_{th}}{\overline{\gamma}_{ub} x}\right) f_{S_{bu}}(x) dx$$
$$= \frac{1}{\theta_{ub}^{\varphi_{ub}}\Gamma(\varphi_{ub})} \sum_{n=1}^{N_{ub}} a_{ub,n} c_{ub,n}^{-b_{ub,n}} \Gamma(b_{ub,n}) \int_0^{+\infty} x^{\varphi_{ub}-1} e^{-x/\theta_{ub}}$$
$$\times \left[1 - e^{-\frac{c_{ub,n}\gamma_{th}}{\overline{\gamma}_{ub}x}} \sum_{m=0}^{b_{ub,n}-1} \frac{1}{m!}\left(\frac{c_{ub,n}\gamma_{th}}{\overline{\gamma}_{ub}x}\right)^m\right] dx. \quad (70)$$

The integral in (70) is computed by using the integral results of $\int_0^{+\infty} t^{\nu-1}e^{-\lambda t}dt = \Gamma(\nu)/\lambda^\nu$ [33, Eq. (3.381.4)] and $\int_0^{+\infty} t^{\nu-1}e^{-\beta/t-\lambda t}dt = 2(\beta/\lambda)^{\nu/2}K_\nu(2\sqrt{\beta\lambda})$, where $K_\nu(.)$ is the ν-th order modified Bessel function of the second kind [33, Eq. (3.478.4)]. After some manipulations, we have

$$Pr(\gamma_{ub} < \gamma_{th}) = \sum_{n=1}^{N_{ub}} a_{ub,n} c_{ub,n}^{-b_{ub,n}} \Gamma(b_{ub,n})\left(1 - \sum_{m=0}^{b_{ub,n}-1} \frac{2}{m!\Gamma(\varphi_{ub})}\right.$$
$$\times \left. \left(\frac{c_{ub,n}\gamma_{th}}{\theta_{ub}\overline{\gamma}_{ub}}\right)^{(\varphi_{ub}+m)/2} K_{\varphi_{ub}-m}\left(2\sqrt{\frac{c_{ub,n}\gamma_{th}}{\theta_{ub}\overline{\gamma}_{ub}}}\right)\right). \quad (71)$$

By substituting the results in (67), (68) and (71) into (30), we obtain the result in (31).

2) High SNR approximation: In the high SNR regime (i.e., $\overline{\gamma}_{ou} \to +\infty, \overline{\gamma}_{ub} \to +\infty$), by using the approximation of the lower incomplete gamma function, we have $\gamma(b_{ou,n}, c_{ou,n}\gamma_{th}/\overline{\gamma}_{ou}) \approx (c_{ou,n}\gamma_{th}/\overline{\gamma}_{ou})^{b_{ou,n}}/b_{ou,n}$ [33, Eq. (8.354.1)]. After some manipulations, we arrive at (cf. (66))

$$Pr(\gamma_{ou} < \gamma_{th}) \approx \sum_{n=1}^{N_{ou}} \frac{a_{ou,n}}{b_{ou,n}} \left(\frac{\gamma_{th}}{\overline{\gamma}_{ou}} \right)^{b_{ou,n}}. \tag{72}$$

Additionally, we can approximate the function $K_{\varphi_{ub}-m}\left(2\sqrt{\frac{c_{ub,n}\gamma_{th}}{\theta_{ub}\overline{\gamma}_{ub}}}\right)$ when $\overline{\gamma}_{ub} \to +\infty$. In particular, we have [45]

$$Pr(\gamma_{ub} < \gamma_{th}) \approx \sum_{n=1}^{N_{ub}} a_{ub,n} c_{ub,n}^{-b_{ub,n}} \Gamma(b_{ub,n}) \left(1 - \sum_{m=0}^{b_{ub,n}-1} \frac{\Gamma(\varphi_{ub}-m)}{m!\Gamma(\varphi_{ub})}\right.$$
$$\left.\times \left(\frac{c_{ub,n}\gamma_{th}}{\theta_{ub}\overline{\gamma}_{ub}}\right)^m \left(1 - \frac{c_{ub,n}\gamma_{th}}{(\varphi_{ub}-m-1)\theta_{ub}\overline{\gamma}_{ub}}\right)\right). \tag{73}$$

Substituting the results in (68), (72) and (73) into (30), we arrive at the result in (32).

APPENDIX E
DERIVATION OF ERGODIC CAPACITIES

1) Exact expression of ergodic capacities: We first calculate the ergodic capacity C_{ou}. From (35), we arrive at

$$C_{ou} = \int_0^{+\infty} \log_2(1+x) f_{\gamma_{ou}}(x) dx, \tag{74}$$

where $f_{\gamma_{ou}}(x)$ is the PDF of the SNR γ_{ou} at the UAV (cf. (6)). Recall that the composite fading $S_{ou}^1 H_{ou}^1$ follows the lognormal-Nakagami-m distribution. Thus, by using the mixture gamma approximation in Section IV.A, we have

$$f_{\gamma_{ou}}(x) = \sum_{n=1}^{N_{ou}} \frac{a_{ou,n}}{\overline{\gamma}_{ou}^{b_{ou,n}}} x^{b_{ou,n}-1} e^{-\frac{c_{ou,n}x}{\overline{\gamma}_{ou}}}. \tag{75}$$

Upon substituting (75) into (74), we have

$$C_{ou} = \sum_{n=1}^{N_{ou}} \frac{a_{ou,n}}{\ln 2 \overline{\gamma}_{ou}^{b_{ou,n}}} \int_0^{+\infty} x^{b_{ou,n}-1} e^{-\frac{c_{ou,n}x}{\overline{\gamma}_{ou}}} \ln(1+x) dx. \tag{76}$$

The integral in (76) is solved by using the results in [46, Eq. (32), Eq. (78)]. After some manipulations, we obtain (37).

Regarding the capacity C_{ub}, from (36) we have

$$C_{ub} = \int_0^{+\infty} \log_2(1+x) f_{\gamma_{ub}}(x) dx, \tag{77}$$

where $f_{\gamma_{ub}}(x)$ is the PDF of the SNR γ_{ub} at the GS (cf. (7)), which is expressed as

$$f_{\gamma_{ub}}(x) = \frac{\partial F_{\gamma_{ub}}(x)}{\partial x} = \frac{\partial}{\partial x} Pr(\gamma_{ub} < x), \tag{78}$$

where $Pr(\gamma_{ub} < x)$ is given in (71). By taking the first-order derivative in (78) and using the result of $\partial(z^v K_v(z))/\partial z = -z^v K_{v-1}(z)$ [33, Eq. (8.486.14)], we obtain

$$f_{\gamma_{ub}}(x) = \sum_{n=1}^{N_{ub}} a_{ub,n} c_{ub,n}^{-b_{ub,n}} \Gamma(b_{ub,n}) \sum_{m=0}^{b_{ub,n}-1} \frac{2}{m!\Gamma(\varphi_{ub})} \times$$
$$\left(\frac{c_{ub,n}}{\theta_{ub}\overline{\gamma}_{ub}}\right)^{\frac{\varphi_{ub}+m}{2}} \left[-mx^{\frac{\varphi_{ub}+m-2}{2}} K_{\varphi_{ub}-m}\left(2\sqrt{\frac{c_{ub,n}x}{\theta_{ub}\overline{\gamma}_{ub}}}\right)\right.$$
$$\left.+\sqrt{\frac{c_{ub,n}}{\theta_{ub}\overline{\gamma}_{ub}}} x^{\frac{\varphi_{ub}+m-1}{2}} K_{\varphi_{ub}-m-1}\left(2\sqrt{\frac{c_{ub,n}x}{\theta_{ub}\overline{\gamma}_{ub}}}\right)\right], \tag{79}$$

where $K_\nu(.)$ is the ν-th order modified Bessel function of the second kind. Substituting (79) into (77), we have

$$C_{ub} = \sum_{n=1}^{N_{ub}} a_{ub,n} c_{ub,n}^{-b_{ub,n}} \Gamma(b_{ub,n}) \sum_{m=0}^{b_{ub,n}-1} \frac{2}{m!\Gamma(\varphi_{ub})\ln 2} \times$$
$$\left(\frac{c_{ub,n}}{\theta_{ub}\overline{\gamma}_{ub}}\right)^{\frac{\varphi_{ub}+m}{2}} \left[-m\mathfrak{I}\left(\frac{\varphi_{ub}+m-2}{2}, \varphi_{ub}-m, 2\sqrt{\frac{c_{ub,n}}{\theta_{ub}\overline{\gamma}_{ub}}}\right)\right.$$
$$\left.+\sqrt{\frac{c_{ub,n}}{\theta_{ub}\overline{\gamma}_{ub}}} \mathfrak{I}\left(\frac{\varphi_{ub}+m-1}{2}, \varphi_{ub}-m-1, 2\sqrt{\frac{c_{ub,n}}{\theta_{ub}\overline{\gamma}_{ub}}}\right)\right], \tag{80}$$

where $\mathfrak{I}(p,q,u) \triangleq \int_0^{+\infty} x^p K_q(u\sqrt{x})\ln(1+x)dx$. The integral $\mathfrak{I}$ is computed by first expressing the logarithmic function in terms of the Meijer-G function, i.e., $\log(1+z) = G_{2,2}^{1,2}\left(z \left| \begin{matrix} 1, & 1 \\ 1, & 0 \end{matrix} \right.\right)$ [47, Chapter 2], and then using the equations in [33, Eq. (7.821.3)] and [33, Eq. (9.31.5)]. After some manipulations, we obtain the expression of C_{ub} in (38).

2) High SNR approximation: In the high SNR regime, we can apply the approximation of $\log(1+x) \approx \log(x)$ when $x \to +\infty$. In particular, (76) can be rewritten as

$$C_{ou} \approx \sum_{n=1}^{N_{ou}} \frac{a_{ou,n}}{\ln 2 \overline{\gamma}_{ou}^{b_{ou,n}}} \int_0^{+\infty} x^{b_{ou,n}-1} e^{-\frac{c_{ou,n}x}{\overline{\gamma}_{ou}}} \ln(x)dx. \tag{81}$$

With the help of the integral result of $\int_0^{+\infty} t^{n-1}\ln(t)e^{-\lambda t}dt = \frac{1}{\lambda^n}\Gamma(n)[\psi(n) - \ln(\lambda)]$ [33, Eq. (4.352.1)], the closed-form expression of C_{ou} is obtained in (39). With respect to the approximation of C_{ub}, we have

$$C_{ub} \approx \sum_{n=1}^{N_{ub}} a_{ub,n} c_{ub,n}^{-b_{ub,n}} (b_{ub,n}-1)! \sum_{m=0}^{b_{ub,n}-1} \frac{2}{m!\Gamma(\varphi_{ub})\ln 2} \times$$
$$\left(\frac{c_{ub,n}}{\theta_{ub}\overline{\gamma}_{ub}}\right)^{\frac{\varphi_{ub}+m}{2}} \left[-m\mathfrak{U}\left(\frac{\varphi_{ub}+m-2}{2}, \varphi_{ub}-m, 2\sqrt{\frac{c_{ub,n}}{\theta_{ub}\overline{\gamma}_{ub}}}\right)\right.$$
$$\left.+\sqrt{\frac{c_{ub,n}}{\theta_{ub}\overline{\gamma}_{ub}}} \mathfrak{U}\left(\frac{\varphi_{ub}+m-1}{2}, \varphi_{ub}-m-1, 2\sqrt{\frac{c_{ub,n}}{\theta_{ub}\overline{\gamma}_{ub}}}\right)\right], \tag{82}$$

where $\mathfrak{U}(p,q,u) \triangleq \int_0^{+\infty} x^p K_q(u\sqrt{x})\ln(x)dx$. To calculate this integral we first change variable $y = \sqrt{x}$ and then use the result in [48, Eq. (2.16.20.1)]. By substituting the obtained expression of $\mathfrak{U}$ into (82) and using the results in [33, Eq. (8.365.4)] and [48, Eq. (2.16.20.1)], we have

$$C_{ub,(m=0)} \approx$$
$$\frac{1}{\ln 2} \sum_{n=1}^{N_{ub}} a_{ub,n} c_{ub,n}^{-b_{ub,n}} \Gamma(b_{ub,n}) \left[\psi(\varphi_{ub}+1) + \psi(1) - \ln\left(\frac{c_{ub,n}}{\theta_{ub}\overline{\gamma}_{ub}}\right)\right], \tag{83}$$

and

$$C_{ub,(m>0)} \approx \frac{1}{\ln 2} \sum_{n=1}^{N_{ub}} a_{ub,n} c_{ub,n}^{-b_{ub,n}} \Gamma(b_{ub,n}) \sum_{m=1}^{b_{ub,n}-1} \frac{1}{m}. \quad (84)$$

Finally, the capacity C_{ub} is obtained as $C_{ub} = C_{ub,(m=0)} + C_{ub,(m>0)}$, which is given in (40). This completes the proof.

Appendix F
Derivation of optimal energy-harvesting time

For delay-tolerant transmission, the optimal value α^{opt} is obtained by solving the following optimization problem

$$\alpha^{opt} = \arg \max_{0<\alpha<1} \frac{\alpha}{K+2} \min\{C_{ou}, C_{ub}\}, \quad (85)$$

where the capacities C_{ou} and C_{ub} are given in Corollary 3. It is worth noting that C_{ou} is independent of α. Meanwhile, C_{ub} is a function of α. Specifically, we can express

$$C_{ub}(\alpha) = \Phi + \Upsilon \ln\left(\frac{1-\alpha}{\alpha}\right), \quad (86)$$

where Φ and Υ are defined as in (41). From (86), it is readily seen that $C_{ou} \leq C_{ub}$, when $\alpha \leq \overline{\alpha}$ where $\overline{\alpha} \triangleq 1/(1 + e^{(C_{ou}-\Phi)/\Upsilon})$, and otherwise. Thus, in case of $\alpha \leq \overline{\alpha}$, (85) can be rewritten as

$$\alpha^{opt} = \arg \max_{0<\alpha\leq\overline{\alpha}} \frac{\alpha}{K+2} C_{ou}. \quad (87)$$

Since C_{ou} is independent of α, the objective function in (87) is an increasing function w.r.t. α. As a result, the maximal throughput is achieved at $\alpha = \overline{\alpha}$ for $\alpha \leq \overline{\alpha}$. This implies that the optimal value α^{opt} for the problem (85) always occurs in the range $\overline{\alpha} \leq \alpha < 1$. Note that when $\alpha \geq \overline{\alpha}$, we have $C_{ou} \geq C_{ub}$. Therefore, the problem in (85) is equivalent to

$$\alpha^{opt} = \arg \max_{\overline{\alpha}\leq\alpha<1} \frac{\alpha}{K+2} \left[\Phi + \Upsilon \ln\left(\frac{1-\alpha}{\alpha}\right)\right]. \quad (88)$$

This problem is solved by using similar calculation steps as in [49]. The result in (41) is thus obtained.

Acknowledgment

References

[1] F. Khelifi, A. Bradai, A. Benslimane, P. Rawat and M. Atri, "A survey of localization systems in Internet of Things," *Mobile Net. App.*, vol. 24, pp. 761-785, June 2019.

[2] Y. Zhou, L. Liu, L. Wang, N. Hui, X. Cui, J. Wu, Y. Peng, Y. Qi and C. Xing, "Service-aware 6G: An intelligent and open network based on the convergence of communication, computing and caching," *Digital Commun. Net.*, vol. 6, no. 3, pp. 253-260, Aug. 2020.

[3] Y. Zhou, L. Tian, L. Liu and Y. Qi, "Fog computing enabled future mobile communication networks: A convergence of communication and computing," *IEEE Commun. Mag.*, vol. 57, no. 5, pp. 20-27, May 2019.

[4] Z. B. Tariq, D. M. Cheema, M. Z. Kamran and I. H. Naqvi, "Non-GPS positioning systems: A survey," *ACM Comp. Surveys*, vol. 50, no. 4, pp. 1-34, Nov. 2017.

[5] G. Han, J. Jiang, C. Zhang, T. Q. Duong, M. Guizani and G. K. Karagiannidis,, "A survey on mobile anchor node assisted localization in wireless sensor networks," *IEEE Commun. Surveys Tuts.*, vol. 18, no. 3, pp. 2220-2243, 2016.

[6] A. Zanella, "Best practice in RSS measurements and ranging," *IEEE Commun. Surveys Tuts.*, vol. 18, no. 4, pp. 2662-2686, 2016.

[7] N. Patwari, A. O. Hero, M. Perkins, N. S. Correal and R. J. O'Dea, "Relative location estimation in wireless sensor networks," *IEEE Trans. Signal Process.*, vol. 51, no. 8, pp. 2137-2148, Aug. 2003.

[8] H. C. So and L. Lin, "Linear least squares approach for accurate received signal strength based source localization," *IEEE Trans. Signal Process.*, vol. 59, no. 8, pp. 4035-4040, Aug. 2011.

[9] J. Rezazadeh, M. Moradi, A. S. Ismail and E. Dutkiewicz, "Superior path planning mechanism for mobile beacon-assisted localization in wireless sensor networks," *IEEE Sensors Journal*, vol. 14, no. 9, pp. 3052-3064, Sept. 2014.

[10] R. M. Vaghefi and R. M. Buehrer, "Received signal strength-based sensor localization in spatially correlated shadowing," in *Proceedings of IEEE Int. Conf. on Acoustics, Speech and Signal Proc. (ICASSP)*, Vancouver, BC, May 2013, pp. 4076-4080.

[11] M. Mozaffari, W. Saad, M. Bennis, Y.-H. Nam, and M. Debbah, "A tutorial on UAVs for wireless networks: applications, challenges, and open problems," *IEEE Commun. Surveys Tuts.*, vol. 21, no. 3, 2019.

[12] Y. Zeng, R. Zhang and T. J. Lim, "Wireless communications with unmanned aerial vehicles: Opportunities and challenges," *IEEE Commun. Mag.*, vol. 54, no. 5, pp. 36-42, May 2016.

[13] L. R. Varshney, "Transporting information and energy simultaneously," in *Proceedings of IEEE Int. Symp. on Infor. Theory (ISIT) 2008*, Toronto, Canada, July 2008, pp. 1612-1616.

[14] X. Lu, P. Wang, D. Niyato, D. I. Kim and Z. Han, "Wireless networks with RF energy harvesting: A contemporary survey," *IEEE Commun. Surveys Tuts.*, vol. 17, no. 2, pp. 757-789, 2015.

[15] R. Zhang and C. K. Ho, "MIMO broadcasting for simultaneous wireless information and power transfer," *IEEE Trans. Wireless Commun.*, vol. 12, no. 5, pp. 1989-2001, May 2013.

[16] N. P. Le, "Throughput analysis of power-beacon assisted energy harvesting wireless systems over non-identical Nakagami-m fading channels," *IEEE Commun. Letts.*, vol. 22, no. 4, pp. 840-843, Apr. 2018.

[17] A. A. Nasir, X. Zhou, S. Durrani and R. A. Kennedy, "Throughput and ergodic capacity of wireless energy harvesting based DF relaying network," in *Proceedings of IEEE Int. Conf. Commun. (ICC) 2014*, Sydney, Australia, June 2014, pp. 4077-4082.

[18] N. P. Le, "Outage probability analysis in power-beacon assisted energy harvesting cognitive relay wireless networks," *Wireless Commun. and Mob. Comp.*, vol. 2017, pp. 1-15, Sept. 2017.

[19] J. Huang, Y. Zhou, Z. Ning and H. Gharavi, "Wireless power transfer and energy harvesting: Current status and future prospects," *IEEE Wireless Commun.*, vol. 26, no. 4, pp. 163-169, Aug. 2019.

[20] B. Ji, Y. Li, B. Zhou, C. Li, K. Song and H. Wen, "Performance analysis of UAV relay assisted IoT communication network enhanced with energy harvesting," *IEEE Access*, vol. 7, pp. 38738-38747, Mar. 2019.

[21] S. Yin, Y. Zhao, L. Li and F. R. Yu, "UAV-assisted cooperative communications with power-splitting information and power transfer," *IEEE Trans. Green Commun. and Netw.*, vol. 3, no. 4, pp. 1044-1057, Dec. 2019

[22] Y. Liu, M. Qiu, J. Hu and H. Yu, "Incentive UAV-enabled mobile edge computing based on microwave power transmission," *IEEE Access*, vol. 8, pp. 28584-28593, Feb. 2020.

[23] Q. Liu, M. Li, J. Yang, J. Lv, K. Hwang, M. S. Hossain and G. Muhammad, "Joint power and time allocation in energy harvesting of UAV operating system," *Comp. Commun.* vol. 150, pp. 811-817, Jan. 2020.

[24] Q. Liu, J. Wu, P. Xia, S. Zhao, W. Chen, Y. Yang and L. Hanzo, "Charging unplugged: Will distributed laser charging for mobile wireless power transfer work?," *IEEE Veh. Tech. Mag.*, vol. 11, no. 4, pp. 36-45, Dec. 2016.

[25] Z. Gong, C. Li , F. Jiang, R. Su, R. Venkatesan, C. Meng, S. Han, Y. Zhang, S. Liu and K. Ha, "Design, analysis, and eld testing of an innovative drone-assisted zero-conguration localization framework for wireless sensor networks," *IEEE Trans. Veh. Tech.*, vol. 66, no. 11, pp. 10322-10335, July 2017.

[26] H. Sallouha, M. M. Azari, A. Chiumento, and S. Pollin, "Aerial anchors positioning for reliable rss-based outdoor localization in urban environments," *IEEE Wireless Commun. Letts.*, vol. 7, no. 3, pp. 376-379, June 2018.

[27] F. B. Sorbelli, S. K. Das, C. M. Pinotti and S. Silvestri, "Range based algorithms for precise localization of terrestrial objects using a drone," *Pervasive and Mob. Comp.*, vol. 48, pp. 20-42, Aug. 2018.

[28] P. Perazzo, F. B. Sorbelli, M. Conti, G. Dini and C. M. Pinotti, "Drone path planning for secure positioning and secure position verication," *IEEE Trans. Mob. Comp.*, vol. 16, no. 9, pp. 2478-2493, Sept. 2017.

[29] S. A. A. Shahidian and H. Soltanizadeh, "Single-and multi-UAV trajectory control in RF source localization," *Arabian J. for Sci. and Eng.*, vol. 42, no. 2, pp. 459466, Feb. 2017.

[30] Y. Ji, C. Dong, X. Zhu and Q. Wu, "Fair-energy trajectory planning for multi-target positioning based on cooperative unmanned aerial vehicles," *IEEE Access*, vol. 8, pp. 9782-9795, 2020.

[31] F. Demiane, S. Sharafeddine and Omar Farhat, "An optimized UAV trajectory planning for localization in disaster scenarios," *Comp. Net.*, vol. 179, June 2020.

[32] D. Ebrahimi, S. Sharafeddine, P. Ho and C. Assi, "Autonomous UAV trajectory for localizing ground objects: A reinforcement learning approach," *IEEE Trans. Mob. Comp.*, Early Access.

[33] I. S. Gradshteyn and I. M. Ryzhik, *Table of Integrals, Series and Products*, Academic Press, 2007.

[34] R. Sun and D. W. Matolak, "Airground channel characterization for unmanned aircraft systems part II: Hilly and mountainous settings," *IEEE Trans. Veh. Tech.*, vol. 66, no. 3, pp. 1913-1925, Mar. 2017.

[35] C. F. Liew, D. DeLatte, N. Takeishi, and T. Yairi, "Recent developments in aerial robotics: An survey and prototypes overview," arXiv preprint arXiv:1711.10085.

[36] M. Lahmeri, M. A. Kishk, and M. Alouini, "Stochastic geometry-based analysis of airborne base stations with laser-powered UAVs," *IEEE Commun. Lett.*, vol. 24, no. 1, pp. 173-177, Jan. 2020.

[37] T. S. Rappaport, *Wireless Communications, Principles and Practices*, Prentice Hall, 2002.

[38] S. M. Kay, *Fundamentals of Statistical Signal Processing: Estimation Theory*, Prentice-Hall, 1993.

[39] S. Atapattu, C. Tellambura and H. Jiang, "A mixture Gamma distribution to model the SNR of wireless channels," *IEEE Trans. on Wireless Commun.*, vol. 10, no. 12, pp. 4193-4203, Dec. 2011.

[40] P. M. Shankar, "Outage analysis in wireless channels with multiple interferers subject to shadowing and fading using a compound PDF model, *AEU Int. Journal of Elec. and Commun.*, vol. 61, no. 4, pp. 255-261, Apr. 2007.

[41] R. Corless, G. H. Gonnet, D. E. G. Hare, D. J. Jeffrey and D. E. Knuth , "On the Lambert W function," *Advances in Comp. Math.*, pp. 329-359, 1996.

[42] N. Senadhira, S. Durrani, X. Zhou, N. Yang and M. Ding, "Uplink NOMA for cellular-connected UAV: Impact of UAV trajectories and altitude," *IEEE Trans. Commun.*, vol. 68, no. 8, pp. 5242-5258, Aug. 2020.

[43] S. Lee, S. Moon, J. Kim and I. Lee, "Capacity analysis of distributed antenna systems in a composite fading channel," *IEEE Trans. Wireless Commun.*, vol. 11, no. 3, pp. 1076-1086, Mar. 2012.

[44] M. R. Spiegel, *Theory and Problems of Probability and Statistics*, McGraw-Hill, 1992.

[45] https://functions.wolfram.com/Bessel-TypeFunctions/BesselK (accessed May 02, 2020).

[46] M. S. Alouini and A. J. Goldsmith, "Capacity of Rayleigh fading channels under different adaptive transmission and diversity-combining techniques," *IEEE Trans. Veh. Tech.*, vol. 48, no. 4, pp. 1165-1181, July 1999.

[47] A. M. Mathai and R. K. Saxena, *Generalized Hypergeometric Functions with Applications in Statistics and Physical Sciences*, Springer, 1973.

[48] A. P. Prudnikov, I. A. Brychkov and A. P. Marichev, *Integrals and Series: Special Function (vol.2)*, CRC Press, 1986.

[49] C. Zhong, X. Chen, Z. Zhang and K. Karagiannidis, "Wireless powered communications: performance analysis and optimization," *IEEE Trans. Commun.*, vol. 63, no. 12, pp. 5178-5190, Dec. 2015.